Lithosphere, published online on 8 October 2015 as doi:10.1130/L464.1

Timing and rates of Holocene normal faulting along the Black Mountains fault zone, Death Valley, USA

Kurt L. Frankel[1,*], Lewis A. Owen[2,†], James F. Dolan[3], Jeffrey R. Knott[4], Zachery M. Lifton[1], Robert C. Finkel[5], and Thad Wasklewicz[6]

[1]SCHOOL OF EARTH AND ATMOSPHERIC SCIENCES, GEORGIA INSTITUTE OF TECHNOLOGY, ATLANTA, GEORGIA 30332, USA
[2]DEPARTMENT OF GEOLOGY, UNIVERSITY OF CINCINNATI, CINCINNATI, OHIO 45221, USA
[3]DEPARTMENT OF EARTH SCIENCES, UNIVERSITY OF SOUTHERN CALIFORNIA, LOS ANGELES, CALIFORNIA 90089, USA
[4]DEPARTMENT OF GEOLOGICAL SCIENCES, CALIFORNIA STATE UNIVERSITY, FULLERTON, CALIFORNIA 92831, USA
[5]CENTER FOR ACCELERATOR MASS SPECTROMETRY, LAWRENCE LIVERMORE NATIONAL LABORATORY, LIVERMORE, CALIFORNIA 94550, USA
[6]DEPARTMENT OF GEOGRAPHY, EAST CAROLINA UNIVERSITY, GREENVILLE, NORTH CAROLINA 27858, USA

ABSTRACT

Alluvial fans displaced by normal faults of the Black Mountains fault zone at Badwater and Mormon Point in Death Valley were mapped, surveyed, and dated using optically stimulated luminescence (OSL) and ^{10}Be terrestrial cosmogenic nuclide (TCN) methods. Applying TCN methods to Holocene geomorphic surfaces in Death Valley is challenging because sediment flux is slow and complex. However, OSL dating produces consistent surface ages, yielding ages for a regionally recognized surface (Qg3a) of 4.5 ± 1.2 ka at Badwater and 7.0 ± 1.0 ka at Mormon Point. Holocene faults offsetting Qg3a yield horizontal slip rates directed toward 323° of 0.8 +0.3/–0.2 mm/yr and 1.0 ± 0.2 mm/yr for Badwater and Mormon Point, respectively. These slip rates are slower than the ~2 mm/yr dextral slip rate of the southern end of the northern Death Valley fault zone and are half as fast as NNW-oriented horizontal rates documented for the Panamint Valley fault zone. This indicates that additional strain is transferred southwestward from northern Death Valley and Black Mountains fault zones onto the oblique-normal dextral faults of the Panamint Valley fault zone, which is consistent with published geodetic modeling showing that current opening rates of central Death Valley along the Black Mountains fault zone are about three times slower than for Panamint Valley. This suggests that less than half of the geodetically determined ~9–12 mm/yr of right-lateral shear across the region at the latitude of central Death Valley is accommodated by slip on well-defined faults and that distributed deformational processes take up the remainder of this slip transferred between the major faults north of the Garlock fault.

LITHOSPHERE doi:10.1130/L464.1

INTRODUCTION

Death Valley constitutes one of the most dramatic landscapes in North America, and it is famous for its faulted mountain fronts, spectacular alluvial fans, and extensive saline playa. Moreover, the valley is the type example of a pull-apart basin (Burchfiel and Stewart, 1966), which is controlled by the NW-trending, right-lateral, strike-slip northern Death Valley–Fish Lake Valley fault zone, the N-trending normal faults of the Black Mountains fault zone, and the NW-trending, right-lateral, strike-slip southern Death Valley fault zone (Fig. 1; Machette et al., 2001). These three fault zones make up the Holocene fault zones of the Death Valley fault system. The Death Valley pull-apart often provides an analog for the evolution, including stress transfer and depositional systems, in other tectonically active transtensional regimes, such as the Dead Sea, East Africa, and Alpine fault of New Zealand (see Mann, 2008).

Late Quaternary deformation rates throughout the Eastern California shear zone (Fig. 1), including the Death Valley fault system, are keys to understanding the strain partitioning across the Pacific–North American plate boundary (Wright, 1976; Dixon et al., 1995; Reheis and Dixon, 1996; Frankel et al., 2007a, 2007b, 2011; Ganev et al., 2010). Variation in the spatial and temporal deformation patterns is critical for understanding how strain is stored and released and provides basic constraints for seismic hazard assessment and tectonic and geomorphic models of the North American plate-boundary evolution. This knowledge may serve as an analog for similar plate boundaries (e.g., Eurasia-Anatolia in Turkey).

Several studies have quantified late Quaternary deformation along the northern Death Valley fault zone (e.g., Klinger, 2001b; Frankel et al., 2007a, b, 2011). Deformation rates along the southern Death Valley fault zone, however, are limited to regional estimates (e.g., Wesnousky, 1986; Butler et al., 1988). Late Quaternary deformation rates for the Black Mountains fault zone are more common than the southern Death Valley fault zone, but these studies either lack numerical dating (Klinger and Piety, 2001), do not extend to the Holocene (Hayman et al., 2003), or are hampered by the structurally segmented nature of the fault zone (Fig. 2; Machette et al., 2001). In this paper, we determined the normal component of late Quaternary deformation along two sections of the Black Mountains fault zone by mapping and numerically dating offset late Quaternary deposits. We use these data to help illustrate the importance of normal faults in the development of the Death Valley basin, as well as their contribution to deformation within the Eastern California shear zone and extension within the Basin and Range.

GEOLOGIC CONTEXT

Death Valley is the hottest place on Earth (maximum recorded temperatures of 56.7 °C at Furnace Creek on 13 July 1913; average annual temperature of 24.8 °C) and the lowest point in North America (85.5 m below sea level at Badwater). Within the rain shadow of the Sierra Nevada, Inyo Mountains, and Panamint Mountains, the average annual precipitation of 48 mm produces a hyperarid climate (geomaps.wr.usgs.gov/parks/deva

*Deceased
†Corresponding author: lewis.owen@uc.edu.

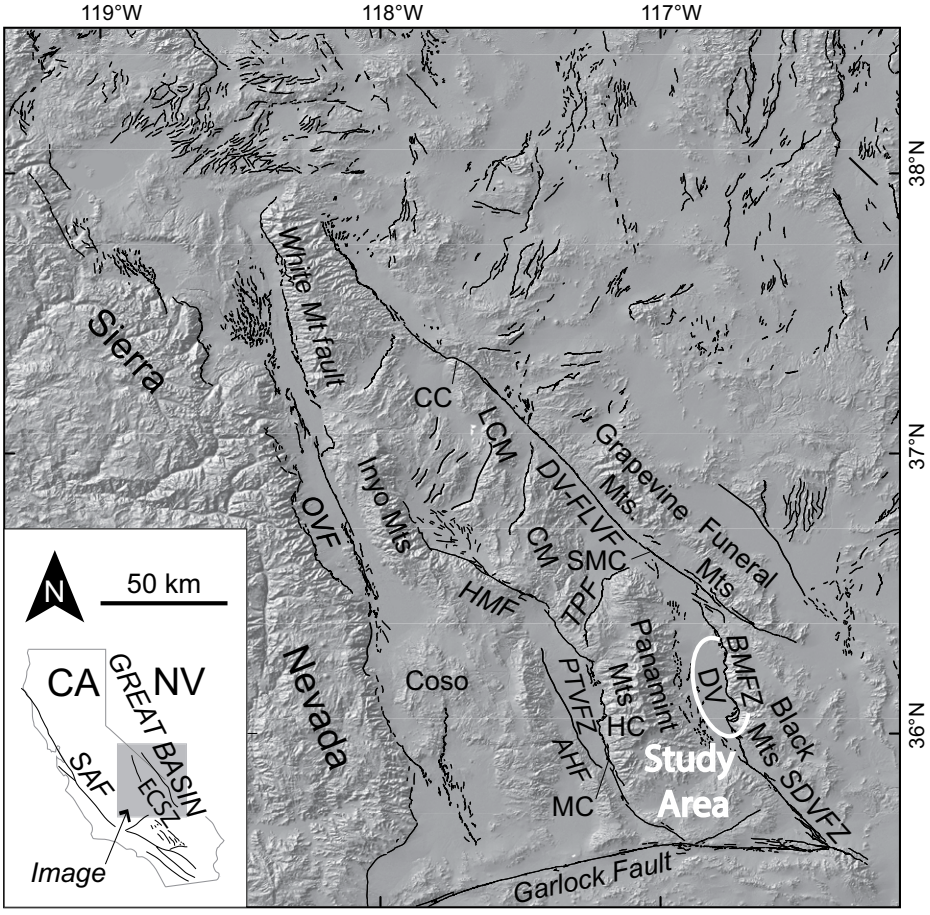

Figure 1. Location of study area showing major faults in the Eastern California shear zone (ECSZ) and westernmost Basin and Range Province (adapted from Frankel et al., 2011); white ellipse is the approximate study area. AHF—Ash Hill fault, BMFZ—Black Mountains fault zone, CA—California, CC—Cucomongo Canyon, CM—Cottonwood Mountains, DV—Death Valley, HC—Happy Canyon, HMF—Hunter Mountain Fault, LCM—Last Chance Mountains, MC—Manly Canyon, DV-FLVF—Death Valley–Fish Lake Valley fault (northern Death Valley fault zone), OVF—Owens Valley fault, NV—Nevada, PTVFZ—Panamint Valley fault zone, SAF—San Andreas fault, SDVFZ—southern Death Valley fault zone, SMC—South Mud Canyon, TPF—Towne Pass fault.

/weather.html). The Panamint Range, Cottonwood Mountains, and Last Chance Range bound Death Valley to the west, and the Grapevine, Funeral, and Black Mountains define Death Valley's eastern margin (Figs. 1 and 2). The diverse bedrock types range in age from Proterozoic to Cenozoic and include metamorphic crystalline basement, quartzite, limestone, dolomite, and sedimentary siliciclastic rocks, along with a wide variety of igneous rocks and volcanic ashes (Hunt and Mabey, 1966). Deeply incised canyons exiting the sparsely vegetated, colluvium-mantled, or bare bedrock slopes of the mountain ranges produce extensive, bajada-forming alluvial fans that surround a saline playa. Death Valley is internally drained, with the Amargosa River reaching the saline playa only during wetter years. Geomorphic, sedimentological, and geochemical evidence suggests that perennial lakes existed in Death Valley during wetter, cooler, late Quaternary glacial times, for example, ca. 120–186 ka and 10–35 ka (Li et al., 1996; Lowenstein et al., 1999; Owen et al., 2011).

Death Valley is located in the southwestern United States, near the western margin of the Great Basin and within the transition between the extensional Basin and Range Province and the dextral strike-slip Eastern California shear zone (Fig. 1). Geodetically, Death Valley is situated within the Western Great Basin Province of Bennett et al. (2003) between the Sierra Nevada–Great Valley and the Central Great Basin Provinces (Fig. 1). The relative motion between Sierra Nevada–Great Valley and Central Great Basin is 9–12 mm/yr toward N37°W (323°; Bennett et al., 2003; Meade and Hager, 2005). This motion is accommodated by a number of NW-SE–trending strike-slip faults and NE-SW–trending normal faults (Fig. 1; e.g., DeMets and Dixon, 1999; Dixon et al., 1995; Reheis and Dixon, 1996).

The classic Death Valley alluvial fans were examined during the early seminal work on these landforms (e.g., Denny, 1965; Hunt and Mabey, 1966; Bull, 1968). Numerous subsequent studies were undertaken of the alluvial-fan stratigraphy and geomorphology (Reynolds, 1969; Hooke, 1972; Bull, 1991; Hooke and Dorn, 1992; Klinger, 2001a, 2001b, 2001c; Machette et al., 2001, 2008; Menges et al., 2001; Knott et al., 1999, 2005; Staley et al., 2006; Volker et al., 2007; Frankel and Dolan, 2007; Wasklewicz et al., 2008). These studies established a geomorphology-based alluvial-fan nomenclature (e.g., Menges et al., 2001) that was subsequently supplemented by optically stimulated luminescence (OSL) and terrestrial cosmogenic nuclide (TCN) surface exposure dating methods (e.g., Nishiizumi et al., 1993; Frankel et al., 2007a, 2007b, 2011; Sohn et al., 2007; Machette et al., 2008; Owen et al., 2011; Fig. 3).

Brogan et al. (1991) mapped fault scarps offsetting alluvial fans for 65 km along the Black Mountains fault zone from Furnace Creek in the north southward to Shoreline Butte. These scarps record possibly three post-Pleistocene ground-rupturing earthquakes with predominantly normal displacement and 0.15–15 m of vertical separation (Brogan et al., 1991; Klinger and Piety, 1996). The Black Mountains fault zone, however, has not generated any historical, surface-rupturing earthquakes (Rogers et al., 1991). Frankel et al. (2001) measured 21 scarp profiles with at least three different scarp morphologies at 11 locations along the Black Mountains fault zone, which they interpreted as late, middle, and early Holocene faulting events. Their results suggested that only a portion the Black Mountains fault zone has ruptured during the Holocene.

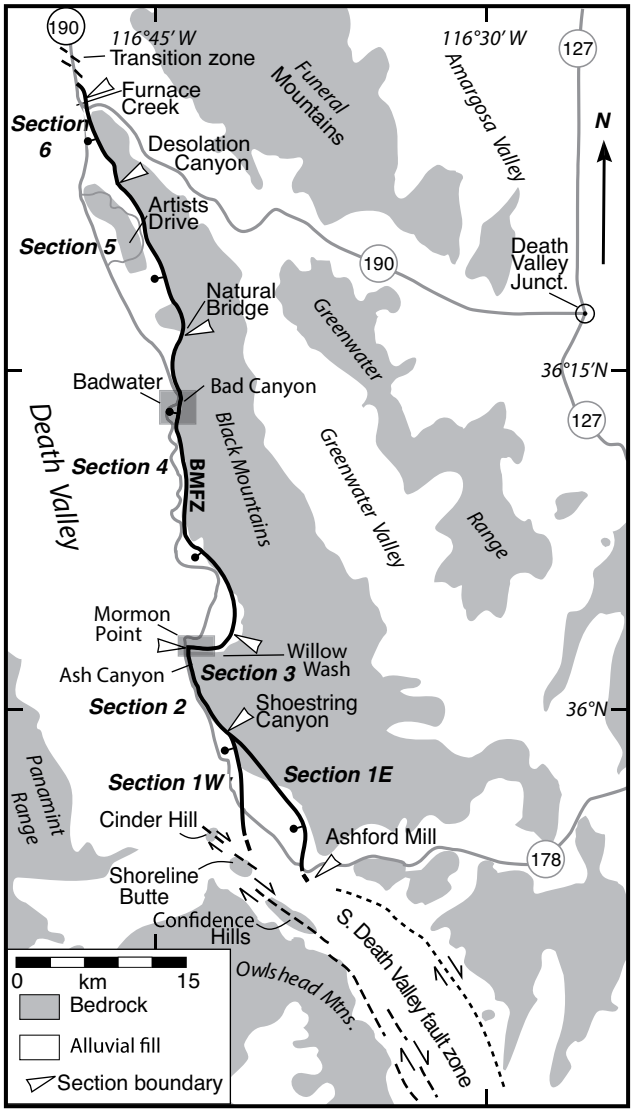

Figure 2. Map of the Black Mountains fault zone (BMFZ) showing geomorphic sections (after Machette et al., 2001). The gray boxes are the approximate study sites at Badwater (Fig. 4) and Mormon Point (Fig. 5).

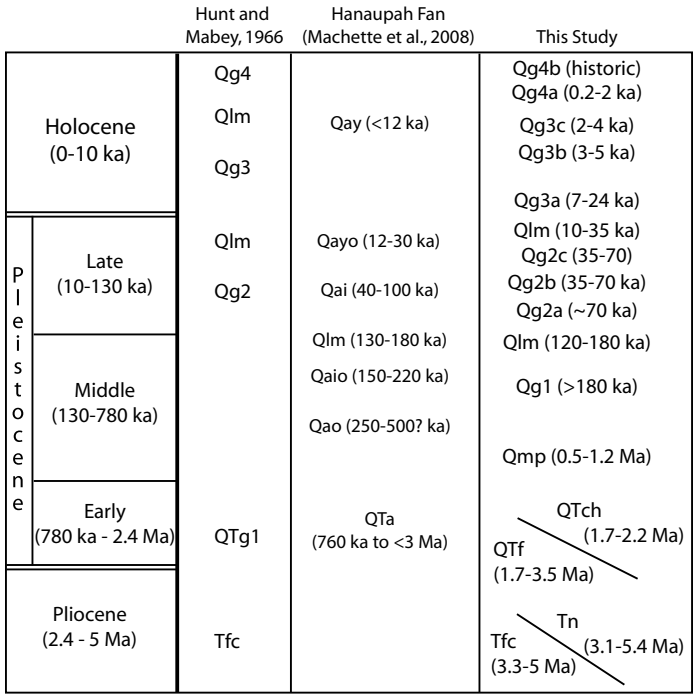

Figure 3. Chart comparing late Neogene formations and map units of Hunt and Mabey (1966), Machette et al. (2008), and this study. Abbreviations for Hunt and Mabey (1966) and this study: Quaternary alluvial-fan gravels (Qg); Lake Manly deposits (Qlm); Mormon Point Formation (Qmp); Confidence Hills Formation (QTch); Funeral Formation (QTf); Nova Formation (Tn); and Furnace Creek Formation (Tfc). Abbreviations for Machette et al. (2008): Quaternary alluvium (Qa), younger (y); intermediate (i), and older (o); Pleistocene-Pliocene alluvium (QTa).

Machette et al. (2001) separated the Black Mountains fault zone into six geomorphic fault sections, which they numbered section 1 (south) to section 6 (north; Fig. 2). Because the Black Mountains fault zone is within Death Valley National Park, paleoseismic studies are limited to natural outcrops; this lack of paleoseismic data results in the use of the fault section terminology rather than fault segments. Working along section 1W south of Mormon Point, Sohn et al. (2014) used crosscutting relations to show the 4–9 ka, OSL-dated Qg3b alluvial fan was offset by three Holocene-age, ground-rupturing earthquakes, as hypothesized by Brogan et al. (1991) and Frankel et al. (2001). Along south-central section 3 (Fig. 2), Klinger and Piety (2001) measured 10.5 m and 4.9 m vertical offsets of the 4–8 ka, soil development–dated Qg3b (Qg3 of Klinger and Piety, 2001) alluvial-fan deposits at Willow Wash and Mormon Point, respectively. Klinger and Piety (2001) estimated a Holocene slip rate of 1–3 mm/yr; however, scarp profiles were complicated by development of calcic and natric soil horizons. Along section 6, at the northern end of the Black Mountains fault zone and the transition zone to the northern Death Valley fault zone (Fig. 2), Machette and Crone (2001) estimated from scarp morphology that the mid-Holocene Qg3c surface was offset by a ground-rupturing earthquake ~600 yr ago.

METHODS

Field Mapping

Geomorphic mapping was undertaken in the field, aided by black-and-white aerial photography, Google Earth imagery, and light detection and ranging (LiDAR)–derived topographic base maps focusing on faulted alluvial fans at Badwater and Mormon Point along the Black Mountains fault zone (Figs. 2–5). We use the nomenclature of Hunt and Mabey (1966) to define the alluvial-fan surfaces and underlying deposits (e.g., Qg1, Qg2, Qg3, Qg4, from oldest to youngest; Fig. 3). Klinger and Sarna-Wojcicki (2001) defined subdivisions of many of these units (e.g., Qg2a, Qg2b), with beginning letters of the alphabet being older. The basis for the subdivision is a combination of rock varnish cover, desert pavement development, height above the active channel, and, where possible, soil development. Similar geomorphic units using a similar nomenclature are described throughout the southwestern United States (Bull, 1991). Because of the previous mapping and regional correlation, we chose this particular nomenclature rather than other mapping units (e.g., Hooke, 1972; Brogan et al., 1991; Menges et al., 2001; Machette et al., 2008).

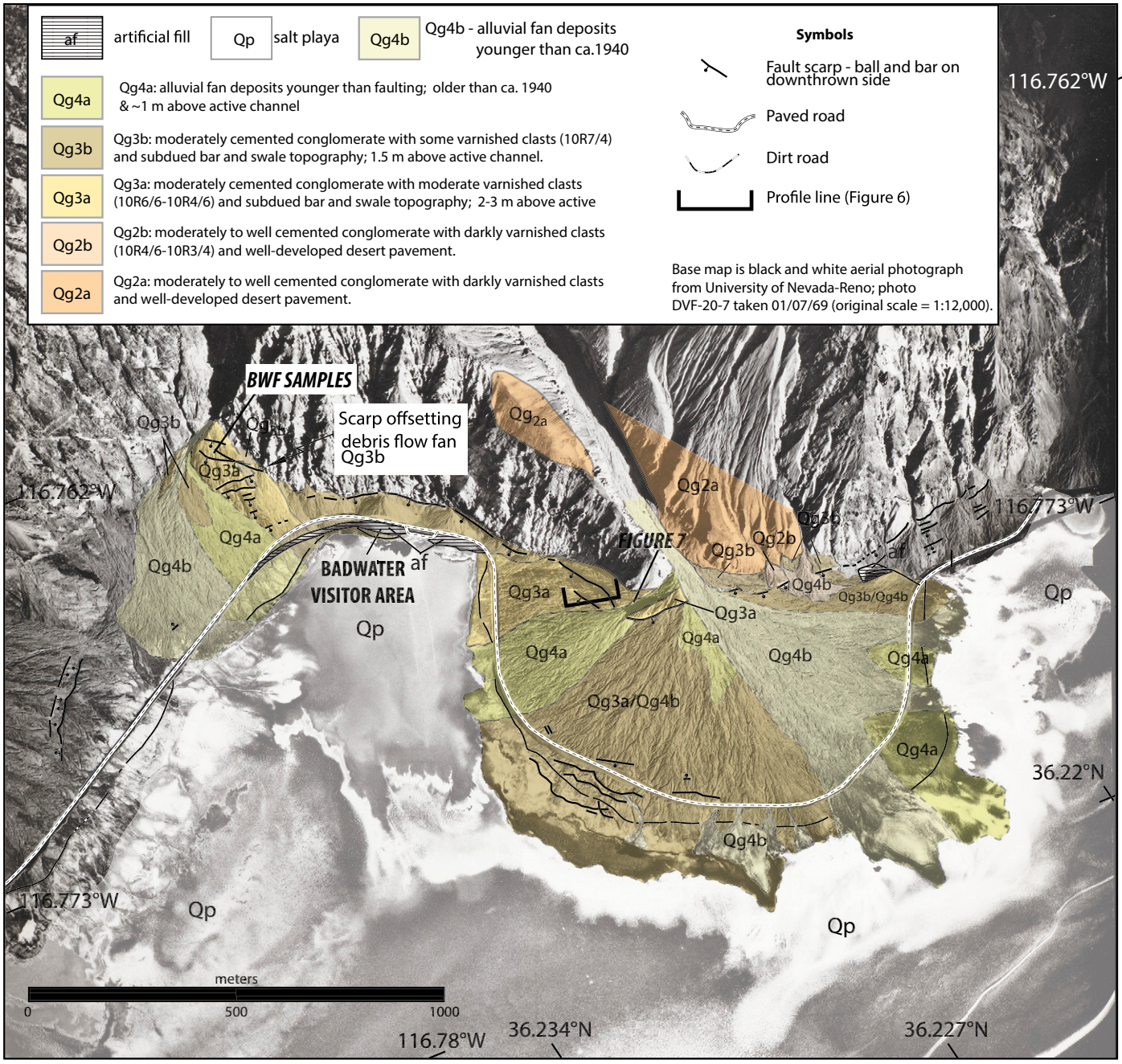

Figure 4. Geomorphic map of the Badwater area. Note locations of light detection and ranging (LiDAR)–based scarp profiles (Fig. 6A) and photographs of Badwater fan sampling location (Fig. 7). The Qg4b alluvial-fan unit buries the dirt road that was abandoned ~75 yr ago (ca. 1940) north of the Badwater visitor area and on the south side of Badwater fan (BWF).

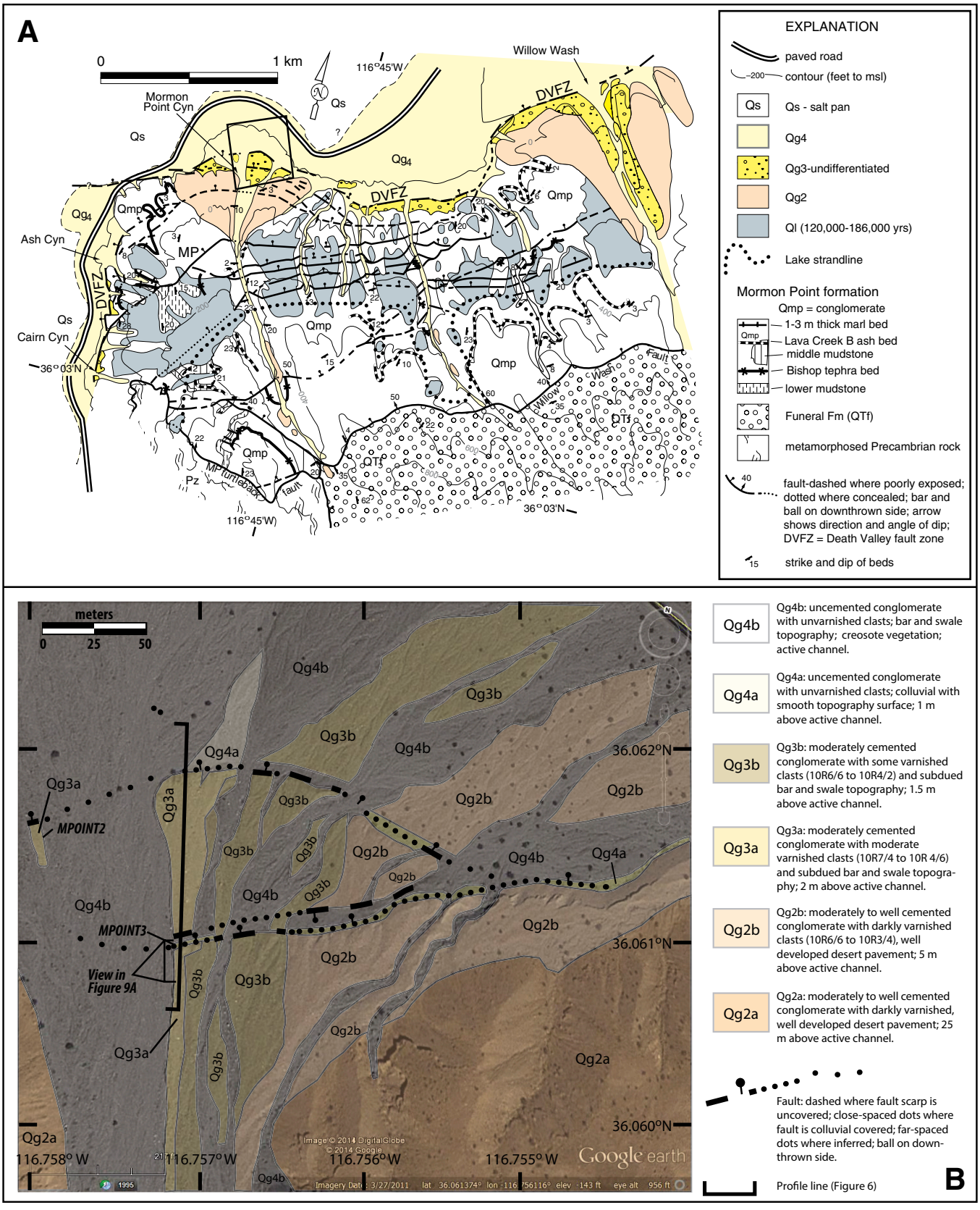

Figure 5. (A) Geologic map of the Mormon Point (MP) area (after Knott et al., 2002); and (B) geomorphic map of Holocene Black Mountains fault zone showing locations of samples and the light detection and ranging (LiDAR)–based topographic profile across the northern and southern strand fault scarps across Qg3a fan surface (Fig. 6A).

Fault Scarp Morphology

We measured the vertical component of fault displacement of the Qg3a fan at Badwater and Mormon Point using digital elevation models (DEMs) derived from airborne LiDAR data. The LiDAR data were collected on three flights between 29 May 2003 and 3 June 2003 by the National Center for Airborne Laser Mapping (NCALM) using an Optech 2033 Airborne Laser Terrain Mapper. The point cloud has a point density of 1.77 points/m^2, and the derived DEM has a resolution of 1 m. We extracted topographic profiles from the DEM that crossed the fault scarps perpendicular to strike and followed the apex-to-toe fall line of the alluvial fan. We fit a linear regression to the profile points along the footwall and hanging-wall surfaces of each scarp and measured the vertical offset between the projected surfaces at the center of the scarp (Fig. 6A). Extension rates versus a range of possible fault dips are shown at each location in Figure 6B.

^{10}Be TCN Dating

Samples were collected from surface boulders, cobbles, and sediment for ^{10}Be dating (Figs. 7–9). Where possible, large boulders (>1 m high) were preferentially sampled from sites that showed the least evidence of erosion. For these large boulders, ~250 g samples of rock were chiseled off the uppermost ≤5 cm of the boulder tops. Whole cobbles were collected where boulders were absent. The location, geomorphic setting, size, shape, and weathering characteristics of each sample were recorded (Table 1). The inclination from the sampling site to the surrounding horizon was measured to quantify topographic shielding. Approximately 1 kg of sediment was collected from vertical natural exposures at intervals of between 25 and 50 cm to a depth of 210 cm and 150 cm on the Badwater and Mormon Point fans, respectively. At each sampling location, the sample site was either buried, or an attempt was made to return the site to its natural, presampling condition.

Boulder and cobble samples were crushed and sieved to obtain a 250–500 μm size fraction. The sediment samples were sieved to obtain the 250–500 μm size fraction. The 250–500 μm size fraction was processed using four acid leaches: aqua regia for >9 h, two 5% HF/HNO_3 leaches for ~24 h, and one 1% HF/HNO_3 leach for 24 h. Lithium heteropolytungstate heavy liquid separation was applied after the first 5% HF/HNO_3 leach. Atomic absorption spectrometry (AAS) Be carrier was added to the pure quartz. The quartz was dissolved in 49% HF and passed through anion and cation exchange columns along with chemical blanks to extract $Be(OH)_2$. The $Be(OH)_2$ was oxidized through ignition at 750 °C and mixed with Nb powder and loaded in steel targets for the measurement of the ^{10}Be/^{9}Be ratios by accelerator mass spectrometry (AMS). AMS measurements were made at the Center for Accelerator Mass Spectrometer at the Lawrence Livermore National Laboratory. Details for standards, blanks, and age calculations are shown in the footnotes of Table 1.

OSL Dating

Samples were collected from freshly cleaned natural exposures (Figs. 7 and 9). At least 30 cm of sediment were scraped away from the face of each exposure before sampling for OSL dating to minimize the possibility of bleaching of the outer layers of the sediment by sunlight. Opaque plastic tubes, ~20 cm long, were hammered perpendicular into the exposed vertical faces to extract the sediment samples. The tubes were sealed and placed in lightproof photographic bags until the initial processing at the University of Cincinnati. At least 5 cm sections of sediment were removed from both ends of the OSL sampling tube under safe light conditions in the luminescence laboratories. The ends and the middle portion of the samples were dried in an oven at 50 °C. The dry ends (or bulk sediment samples) were crushed, homogenized, and sent to the U.S. Geological Survey Nuclear Reactor facility in Denver for neutron activation analysis to determine radioisotope concentrations following the procedures described in Budahn and Wandless (2002). The middle part of the tube was sieved. The dominant coarse-grained fraction (either 90–125 μm, 125–180 μm, or 180–250 μm) was processed to obtain pure quartz by leaching in 10% HCl for 24 h, 30% H_2O_2 for 24 h, and 10% HF for 20 min, and separation using heavy liquid (lithium polytungstate). The quartz was leached using 49% HF for 40 min to etch the outer 10 μm of each grain and then leached in 10% HCl for 2 h. Steel target discs were sprayed with silica spray, and a single-grain-thick layer of approximately a few hundred quartz grains was dispersed onto the steel discs.

The luminescence signals were measured using a Riso TL/OSL reader (model DA-20). Luminescence from the quartz grains was stimulated using an array of blue-light-emitting diodes (470 nm, 50 mW/cm^2) filtered using a green long-pass GG-420 filter. Detection was through a Hoya U-340 filter. All quartz aliquots were screened for feldspar contamination using infrared stimulation with infrared-light-emitting diodes (870 nm, 150 mW/cm^2). All OSL signals were detected using a 52-mm-diameter photomultiplier tube (9235B). The equivalent dose (D_e) measurements were determined on multiple aliquots using the single aliquot regenerative (SAR) method protocol developed by Murray and Wintle (2000). Growth curve data were fitted using linear and exponential trend curves. The D_e value for every aliquot was examined using Riso Analysis 3.22b software. Between 21 and 54 aliquots were measured per sample. Aliquots with poor recuperation (>10%) were not used in the age calculations. Equivalent doses of all aliquots were averaged for each sample and then divided by the dose rate, giving a mean age (Table 2). Calculation uncertainties and methods used to calculate dose rates are explained in the footnotes in Table 2.

RESULTS

Dating

Concentrations of TCNs in rock and sediment are a function of the time of exposure to cosmic rays and the TCN production rate at the site. Production rate is dependent upon the cosmic-ray flux. This varies spatially and temporally in association with variations in the geomagnetic field intensity and atmospheric pressure throughout the Quaternary. There is much debate regarding the appropriate scaling models and geomagnetic corrections for TCN production to calculate TCN ages (e.g., Pigati and Lifton, 2004; Staiger et al., 2007; Balco et al., 2008). For the latitude and altitudes of Death Valley, the different scaling models yield age differences of ≤15% and ≤10% for the Holocene and late Pleistocene, respectively. We used surface clast ^{10}Be ages calculated using the Lal (1991) and Stone (2000) time-dependent model assuming zero erosion, but we present ages calculated using other models in Table 1 for comparison. The ^{10}Be ages for the Qg3a and Qg4a surfaces are presented, analyzed, and plotted using normal kernel probability density estimates (Fig. 10). The ^{10}Be concentrations for depth profile samples are plotted in Figures 6C and 8E.

The ^{10}Be ages for surface clasts on individual surfaces range from ca. 2–71 ka for the Qg4a fan surface at Badwater to 2–42 ka and 4–48 ka for the Qg3a fan surfaces at Badwater and Mormon Point, respectively (Fig. 10; Table 3). These data highlight the large degree of inheritance of ^{10}Be in surface clasts in this hyperarid region. Considering that the Qg4 surface (active channel) at Badwater buries the dirt road (Fig. 4; see following) abandoned ca. A.D. 1940 (Hunt and Mabey, 1966, p. 93) and is

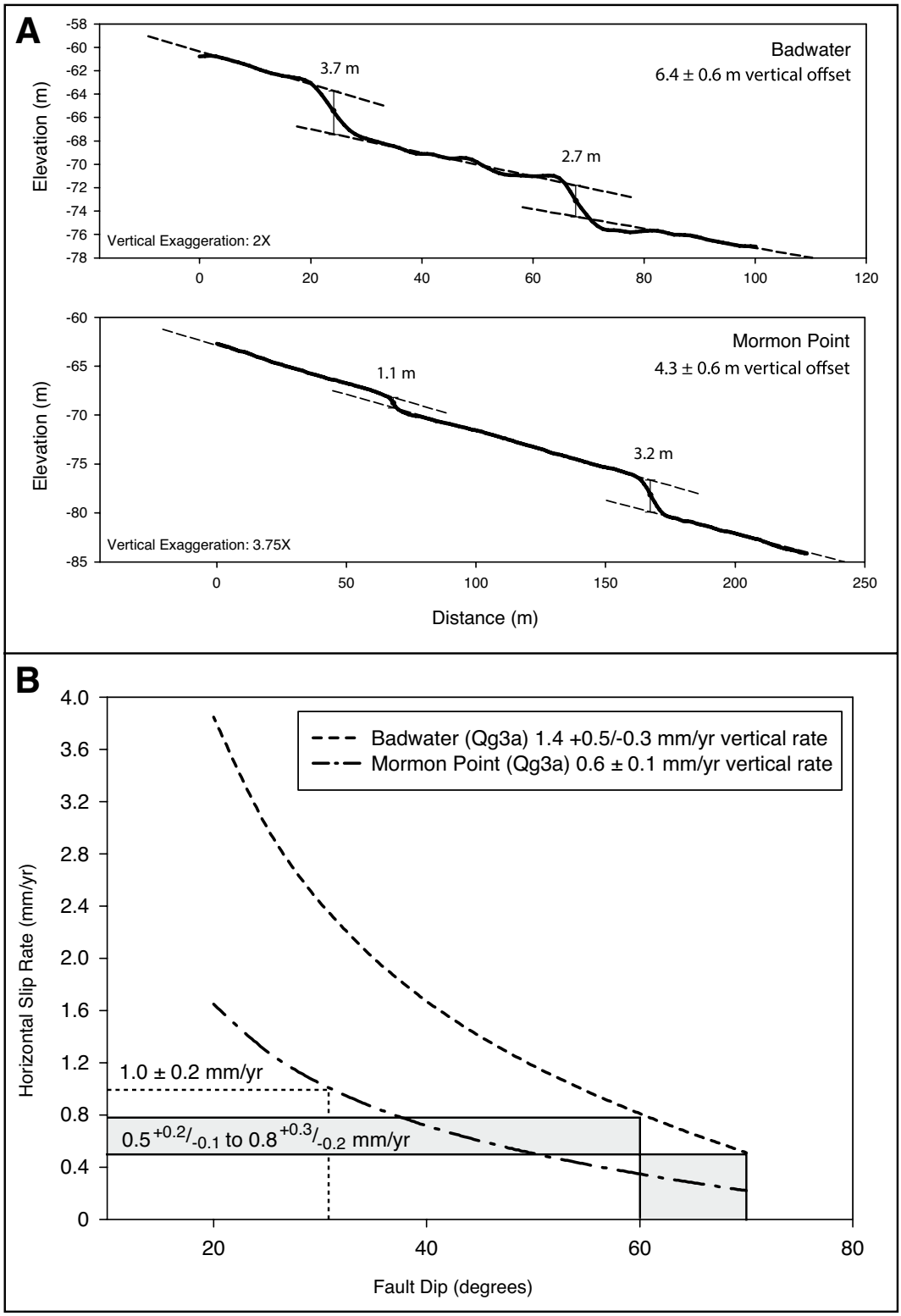

Figure 6. Geomorphic characteristics of fault scarps at Badwater and Mormon Point. (A) Profiles across fault scarps, and (B) extension rate vs. fault dip for vertical slip rates of 1.4 +0.5/–0.3 mm/yr and 0.6 ± 0.1 mm/yr.

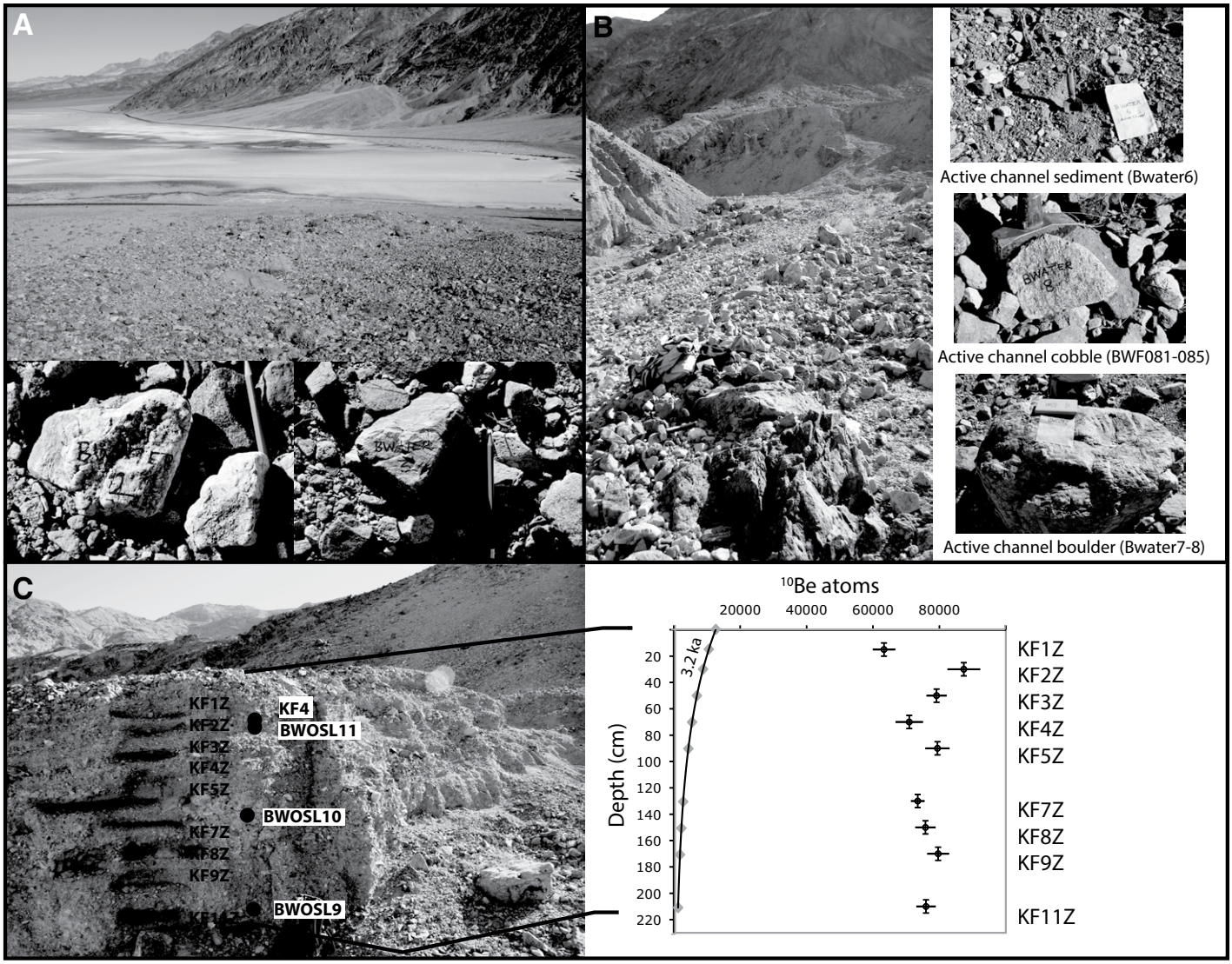

Figure 7. Sampling locations of optically stimulated luminescence (OSL) and terrestrial cosmogenic nuclide (TCN) dating on Qg3a alluvial fan southwest of Badwater visitor's area. (A) View of surface of alluvial fan looking ENE toward Badwater, showing examples of cobbles that were collected for TCN dating (Bwater1 through Bwater5); Badwater visitor's area is just out of view to right of photograph). (B) View looking upstream of active alluvial-fan channel (Qg4), and view of sediment and examples of cobbles and boulders that were collected for TCN dating (Bwater6 through Bwater8, and BWF081 through BWF085). (C) View looking east at channel margin incised into the Qg3a fan showing the location of sampling sites for TCN depth profile and OSL dating; and concentrations of TCNs within the depth profile. The solid curve shows the modeled ^{10}Be concentrations for a fan surface with an age of 3.2 ka (weighted mean of top three OSL samples). The black circles show the location of the OSL samples.

therefore less than 75 yr old, the ca. 2–71 ka age range of ^{10}Be ages is particularly striking, but perhaps not surprising in light of previous suggestions of exceedingly complex inheritance issues in such environments as discussed in Machette et al. (2008) and Owen et al. (2011). Clasts in the active channel are likely derived from the older Qg2 deposits or slopes mantling the canyon wall upstream.

The ^{10}Be concentrations in depth profiles at Badwater and Mormon Point exhibit no systematic exponential decrease with depth (Figs. 7C and 9E), as is theoretically predicted (Anderson et al., 1996). Moreover, the concentrations increase and decrease erratically with depth. This suggests that the sediment comprising the alluvial fans has a complex history of prior exposure. We calculated a hypothetical ^{10}Be depth profile for the two depth profiles using Holocene ages determined by our OSL dating as a comparison (Figs. 7C and 9E). The predicted ^{10}Be concentrations are at least 25% to over an order of magnitude less than those measured. This also reflects considerable inheritance of ^{10}Be within alluvial-fan sediments along the Black Mountains. These results illustrate the challenge of using ^{10}Be methods to date Holocene alluvial fans along the Black Mountains in Death Valley. However, these data also show that sediment may be stored on valley slopes and within valley systems for long periods ($10^{3–4}$ yr) and may undergo multiple periods of reworking and deposition before being deposited in locations where it is sampled.

In contrast, the OSL ages determined on the Qg3a surfaces provide ages that are consistent with the geomorphology and weathering characteristics on these surfaces. All OSL ages are Holocene and are presented in Tables 2 and 3. We take the OSL mean age for samples determined in the

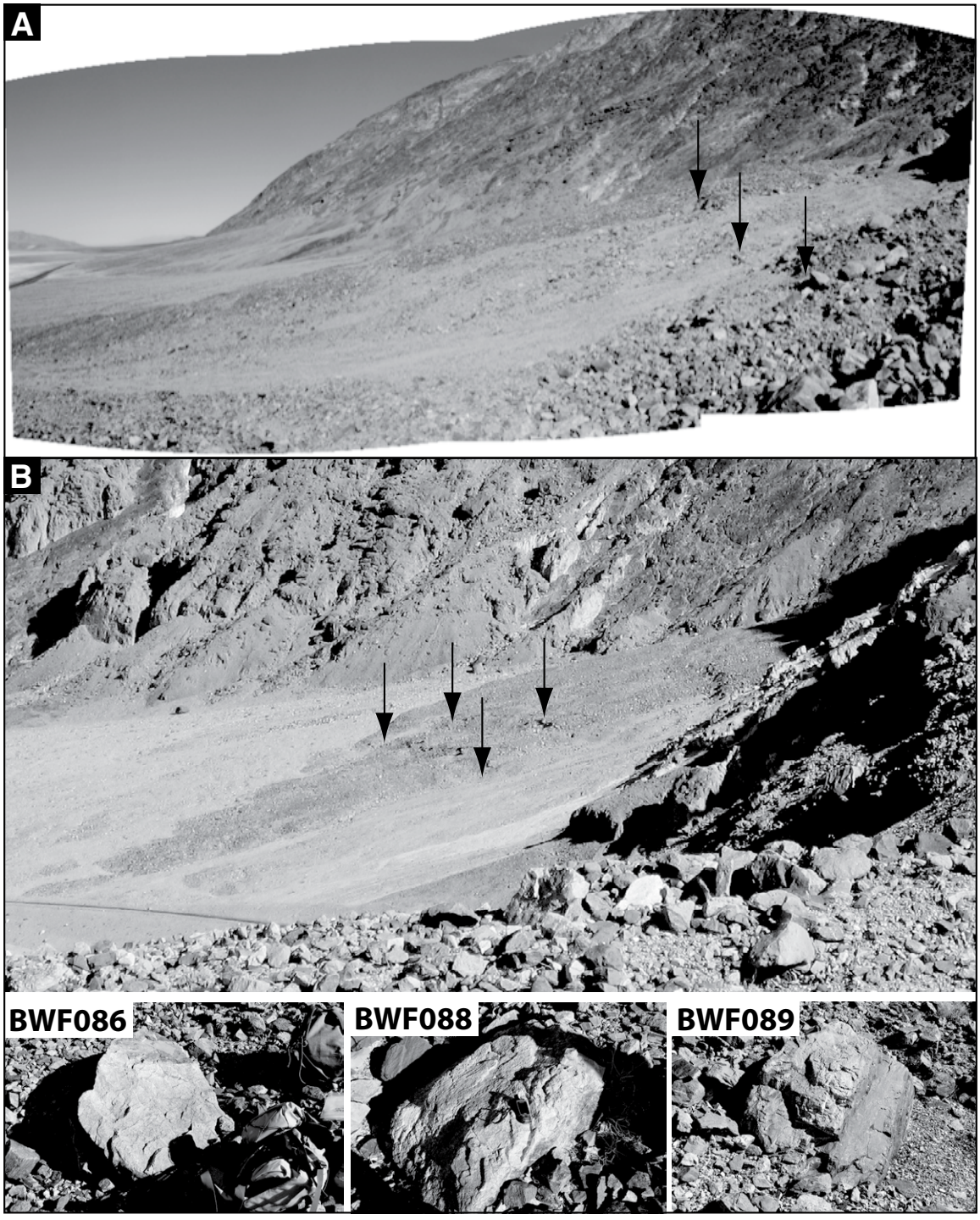

Figure 8. (A) View NE of scarps across Qg3a deposit (left arrow), Qg3b deposit (center arrow), and younger debris fan (right arrow) north of Badwater visitor area. (B) View of small faulted Qg3a alluvial fan east of Badwater showing the boulders that were sampled for TCN dating. The arrows in parts A and B are spaced ~50 m apart. The long axes of boulders BWF086, BWF088 and BWF089 are 140, 135 and 110 cm.

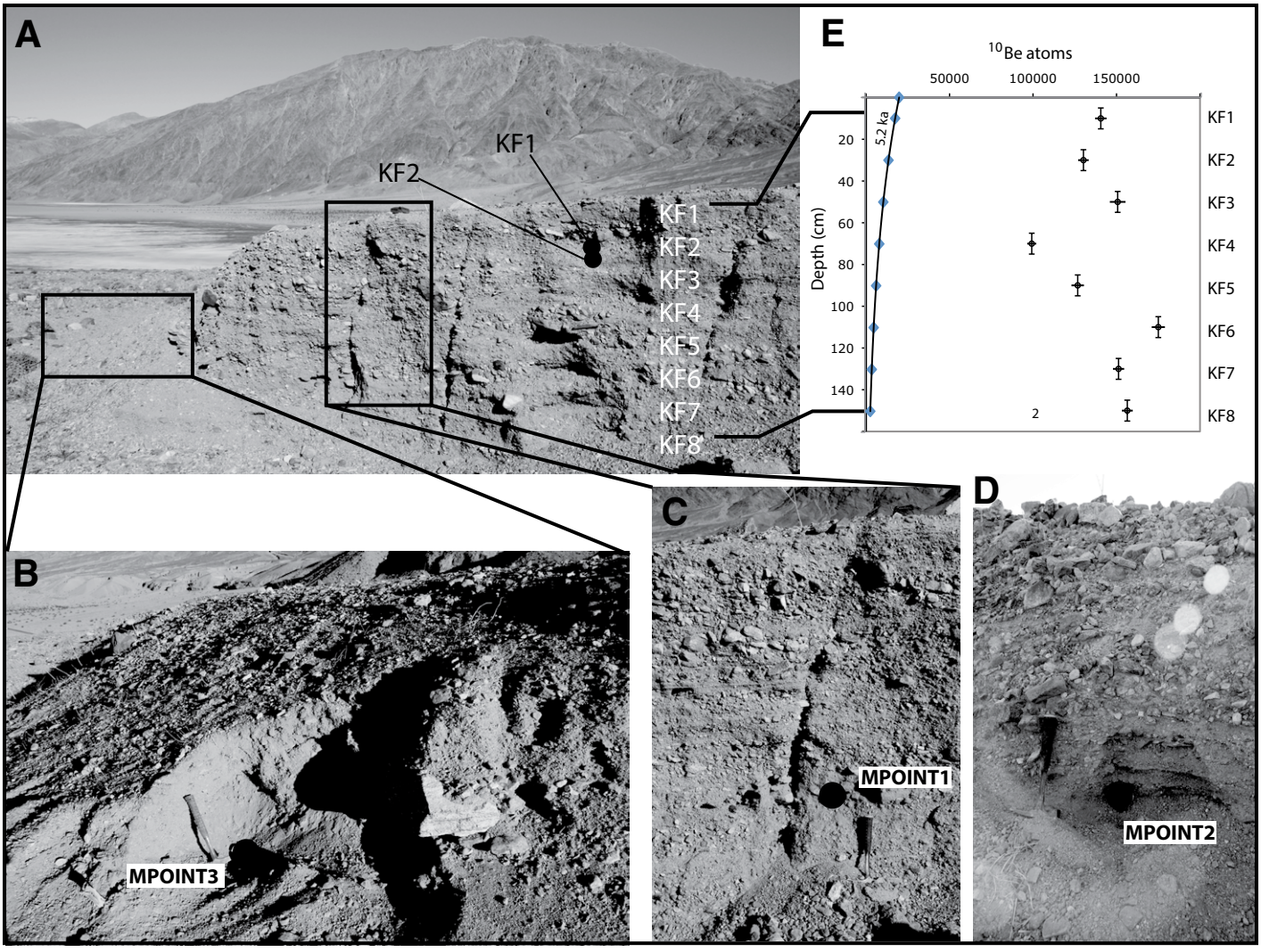

Figure 9. Sampling locations of optically stimulated luminescence (OSL) and terrestrial cosmogenic nuclide (TCN) dating on Qg3a fan at Mormon Point. The black circles show the location of the OSL samples. (A) View looking east at channel margin in the Qg3a fan showing the location of sampling sites for TCN and OSL dating. Note surface scarp of northern fault strand. (B) Colluvial wedge (Qg4a) forming off northern fault strand showing sampling position for OSL sample MPOINT3. (C–D) Detailed views of sample locations for OSL samples MPOINT1 on the east side of the channel (Qg3a) and MPOINT2 on the west side of the channel (Qg3a). (E) Concentrations of TCNs within the depth profile. The solid curve shows the modeled ^{10}Be concentrations for a fan surface with an age of 5.2 ka (youngest OSL age).

upper 2 m of each surface as the maximum age (Qg3a at Badwater = 4.5 ± 1.2 ka; Qg3a at Mormon Point = 7.0 ± 1.1 ka), and hence a maximum age for the faulting that offsets the surfaces. The OSL ages are plotted as normal kernel probability density estimates with the TCN ages for comparison in Figure 11.

Badwater Stratigraphy

Six alluvial-fan deposits were mapped at Badwater (Fig. 4). The older alluvial-fan deposits (Qg2a and Qg2b) typically have darkly varnished clasts and a well-developed desert pavement. The Qg2a deposit is found as uplifted terraces along Bad Canyon more than 25 m above the active channel. The surface of Qg2a is not preserved or exposed within the study area. The other older alluvial-fan deposits (Qg2b), which have darkly varnished clasts (10R 4/6–10R 3/4), are preserved south of the mouth of Bad Canyon. Exposures in stream cuts show a stage II–III pedogenic carbonate morphology (after Machette, 1985) developed on near-surface clasts of the Qg2b deposit.

The intermediate-age alluvial-fan deposits (Qg3a and Qg3b) have subdued bar-and-swale topography. The Qg3a deposit is found 2–3 m above the active channel with varnished clasts of moderate darkness (10R6/6–10R4/6). At Badwater, the ^{10}Be TCN ages for Qg3a range from 9 to 43 ka at Bad Canyon. The probability density plot is similar to the Mormon Point data in that there are a number of peaks that prohibit conclusive interpretation of the data. The OSL ages range from 2.9 to 5.8 ka, with the three lowest samples having ages of 5.1 ka, 5.5 ka, and 5.8 ka. A mean of the six OSL ages is 4.5 ± 1.2 ka (Fig. 11) within the debris-flow fan deposits. The 4.5 ± 1.2 ka age is consistent with the minimum age for Qg3a estimated elsewhere in Death Valley on the basis of soil development (e.g., Klinger and Piety, 2001).

Three boulders were collected for ^{10}Be TCN dating (BWF086, BWF088, and BWF089) on the Qg3a alluvial fan northeast of the Bad-

TABLE 1. ANALYTICAL DATA AND RESULTS FOR ^{10}BE TERRESTRIAL COSMOGENIC GEOCHRONOLOGY

Sample name	Surface	Location		Elevation below sea level (m)	Size *a*/*b*/*c* axes (cm)	Thickness (cm)	Depth (cm)	Production rate (atoms/g SiO_2/yr)		Shielding factor	Denudation rate (mm/yr)	Quartz[§] (g)	Be carrier mass (mg)	Be carrier concentration (µg/g)	$^{10}Be/^{9}Be^{\#,**}$ $\times10^{-13}$	^{10}Be (10^5 atoms/g SiO_2) concentration**,††,§§	Time-independent age, Lal (1991), Stone (2000)$^{**,\#\#,***}$ (ka)	Desilets et al. (2002, 2006) age$^{**,\#\#,***}$ (ka)	Dunai (2001) age$^{**,\#\#,***}$ (ka)	Lifton et al. (2005) age$^{**,\#\#,***}$ (ka)	Time-dependent age Lal (1991), Stone (2000)$^{**,\#\#,***}$ (ka)
		Latitude (°N)	Longitude (°W)					Spallation*	Muons†												
Badwater																					
Bwater1	Qg3a	36.2260	116.7711	19	16.5/11.5/9.5	12.5	0	3.52	0.177	1.00	0	16.9314	0.6281	1155	0.167 ± 0.012	0.414 ± 0.029	10.2 ± 1.1	11.4 ± 1.6	11.1 ± 1.5	11.3 ± 1.4	10.2 ± 1.4
Bwater2	Qg3a	36.2261	116.7711	19	16.5/10.5/7.5	11.5	0	3.54	0.177	1.00	0	27.5000	0.6501	1155	0.456 ± 0.025	0.721 ± 0.040	17.6 ± 1.8	19.5 ± 2.5	18.9 ± 2.5	19.2 ± 2.2	17.6 ± 1.8
Bwater3	Qg3a	36.2261	116.7711	19	21.5/13.5/10.5	15	0	3.45	0.177	1.00	0	22.3018	0.5865	1414	0.217 ± 0.010	0.382 ± 0.017	9.6 ± 0.9	10.7± 1.4	10.5± 1.3	10.6± 1.2	9.6 ± 0.9
Bwater4	Qg3a	36.2262	116.7711	21	12.5/7.5/4.5	8	0	3.64	0.177	1.00	0	29.4267	0.4655	1155	0.170 ± 0.040	1.802 ± 0.043	43.2 ± 3.9	44.8 ± 5.4	44.0 ± 5.3	43.8 ± 4.5	41.7 ± 3.7
Bwater5	Qg3a	36.2262	116.7712	24	12.0/9.0/7.0	9	0	3.31	0.177	0.92	0	5.8538	0.3136	1414	0.181 ± 0.008	0.650 ± 0.029	16.9 ± 1.7	18.7 ± 2.4	18.2 ± 2.3	18.5 ± 2.0	16.9 ± 1.6
Bwater6	Qg4	36.2250	116.7707	10	sediment	5	0	3.77	0.179	1.00	0	21.1839	0.6750	1155	0.371 ± 0.019	0.793 ± 0.041	18.2 ± 1.9	20.1 ± 2.6	19.6 ± 2.5	19.9 ± 2.2	18.2 ± 1.8
Bwater7	Qg4	36.2250	116.7706	13	8.0/8.0/5.0	7	0	3.7	0.178	1.00	0	30.6018	0.4643	1155	0.783 ± 0.019	0.795 ± 0.019	18.6 ± 1.7	20.6 ± 2.5	20.0 ± 2.4	20.3 ± 2.1	18.6 ± 1.6
Bwater8	Qg4	36.2250	116.7706	9	15.0/11.0/3.0	10	0	3.62	0.178	1.00	0	29.5965	0.4824	1155	0.153 ± 0.013	0.166 ± 0.014	4.0 ± 0.5	4.7 ± 0.7	4.6 ± 0.7	4.7 ± 0.6	4.1 ± 0.5
BWF081	Qg4	36.2255	116.7714	17	100/50/25	2	0	3.84	0.179	1.00	0	9.7270	0.4154	1414	1.12 ± 0.026	3.201 ± 0.076	73.4 ± 6.7	76.8 ± 9.4	75.1 ± 9.2	75.2 ± 7.8	71.0 ± 6.3
BWF082	Qg4	36.2253	116.7715	14	160/90/70	2	0	3.85	0.179	1.00	0	21.3774	0.6577	1155	0.234 ± 0.013	0.481 ± 0.028	10.8 ± 1.1	12.2 ± 1.6	11.9 ± 1.6	12.0 ± 1.4	10.9 ± 1.1
BWF083	Qg4	36.2257	116.7712	19	80/60/60	3	0	3.8	0.178	1.00	0	15.3664	0.6448	1155	0.058 ± 0.013	0.163 ± 0.029	3.7 ± 0.7	4.5 ± 1.0	4.3 ± 0.9	4.4 ± 0.9	3.9 ± 0.8
BWF084	Qg4	36.2257	116.7712	20	125/110/60	3	0	3.67	0.178	0.97	0	20.9832	0.5707	1414	0.074 ± 0.005	0.134 ± 0.009	3.2 ± 0.4	3.8 ± 0.5	3.7 ± 0.5	3.8 ± 0.5	3.3 ± 0.4
BWF085	Qg4	36.2261	116.7713	25	160/130/65	3	0	3.78	0.178	1.00	0	16.9663	0.5853	1414	0.037 ± 0.008	0.085 ± 0.018	2.0 ± 0.5	2.4 ± 0.6	2.3 ± 0.6	2.3 ± 0.6	2.0 ± 0.5
BWF086	Qg3a	36.2328	116.7630	19	140/90/60	2.5	0	3.82	0.178	1.00	0	29.6249	0.6004	1155	0.459 ± 0.018	0.623 ± 0.025	14.2 ± 1.4	15.8 ± 2.0	15.4 ± 1.9	15.6 ± 1.7	14.2 ± 1.3
BWF088	Qg3a	36.2328	116.7631	18	135/130/60	4	0	3.77	0.178	1.00	0	21.0776	0.6516	1414	0.037 ± 0.008	0.077 ± 0.016	1.8 ± 0.4	2.1 ± 0.5	2.0 ± 0.5	2.1 ± 0.5	1.8 ± 0.4
BWF089	Qg3a	36.2328	116.7631	22	110/80/90	4	0	3.76	0.178	1.00	0	20.4852	0.6667	1155	0.115 ± 0.014	0.251 ± 0.031	5.8 ± 0.9	6.5 ± 1.1	6.4 ± 1.1	6.5 ± 1.0	5.9 ± 0.9
KF1Z	Qg3a	36.2260	116.7712	21	n/a	0	15	–	–	0.95	0	28.4074	0.6340	1155	0.424 ± 0.023	0.633 ± 0.034	–				
KF2Z	Qg3a	36.2260	116.7712	21	n/a	0	30	–	–	0.93	0	15.0995	0.6536	1155	0.302 ± 0.0170	0.874 ± 0.049	–				
KF3Z	Qg3a	36.2260	116.7712	21	n/a	0	50	–	–	0.93	0	20.8592	0.6002	1414	0.411 ± 0.0158	0.791 ± 0.030	–				
KF4Z	Qg3a	36.2260	116.7712	21	n/a	0	70	–	–	0.98	0	13.2504	0.5730	1414	0.245 ± 0.014	0.709 ± 0.041	–				
KF5Z	Qg3a	36.2260	116.7712	21	n/a	0	90	–	–	0.98	0	18.1424	0.5901	1414	0.365 ± 0.017	0.794 ± 0.037	–				
KF7Z	Qg3a	36.2260	116.7712	21	n/a	0	130	–	–	0.98	0	31.6524	0.5744	1414	0.605 ± 0.017	0.735 ± 0.021	–				
KF8Z	Qg3a	36.2260	116.7712	21	n/a	0	150	–	–	0.98	0	14.8743	0.5547	1414	0.304 ± 0.012	0.758 ± 0.037	–				
KF9Z	Qg3a	36.2260	116.7712	21	n/a	0	170	–	–	1.00	0	24.3530	0.5919	1414	0.490 ± 0.020	0.796 ± 0.033	–				
KF11Z	Qg3a	36.2260	116.7712	21	n/a	0	210	–	–	1.00	0	14.9020	0.5590	1414	0.303 ± 0.012	0.760 ± 0.029	–				
Mormon Point																					
KFMP101	Qg3a	36.0618	116.7564	49	>30 cm diameter	5	0	3.63	0.176	1.00	0	74.9976	0.3106	1000	7.409 ± 0.318	2.053 ± 0.088	49.4 ± 4.8	51.3 ± 6.5	50.2 ± 6.4	50.1 ± 5.5	47.6 ± 4.6
KFMP103	Qg3a	36.0618	116.7564	49	>30 cm diameter	5	0	3.63	0.176	1.00	0	54.2447	0.3080	1000	1.733 ± 0.063	0.658 ± 0.024	15.7 ± 1.5	17.4 ± 2.2	17.0 ± 2.1	17.2 ± 1.8	15.7 ± 1.4
KFMP105	Qg3a	36.0618	116.7564	49	>30 cm diameter	5	0	3.63	0.176	1.00	0	75.0042	0.3103	1000	0.605 ± 0.063	0.167 ± 0.018	4.0 ± 0.5	4.8 ± 0.8	4.6 ± 0.7	4.7 ± 0.7	4.1 ± 0.6
KFMP106	Qg3a	36.0618	116.7564	49	>30 cm diameter	5	0	3.63	0.176	1.00	0	73.7852	0.3090	1000	1.560 ± 0.079	0.437 ± 0.022	10.4 ± 1.0	11.7 ± 1.5	11.4 ± 1.5	11.5 ± 1.3	10.5 ± 1.0
KFMP110	Qg3a	36.0618	116.7564	49	>30 cm diameter	5	0	3.63	0.176	1.00	0	74.9966	0.3088	1000	1.460 ± 0.078	0.401 ± 0.022	9.6 ± 1.0	10.7 ± 1.4	10.5 ± 1.4	10.6 ± 1.2	9.6 ± 1.0
KFMP112	Qg3a	36.0618	116.7564	49	>30 cm diameter	5	0	3.63	0.176	1.00	0	75.0206	0.3081	1000	2.154 ± 0.092	0.592 ± 0.025	14.1 ± 1.4	15.8 ± 2.0	15.3 ± 1.9	15.6 ± 1.7	14.2 ± 1.3
KF1	Qg3a	36.0610	116.7570	38	n/a	0	10	–	–	1.00	0	31.8297	0.4878	1155	1.371 ± 0.034	1.406 ± 0.035	–				
KF2	Qg3a	36.0610	116.7570	38	n/a	0	30	–	–	1.00	0	40.9117	0.4954	1155	1.609 ± 0.039	1.302 ± 0.032	–				
KF3	Qg3a	36.0610	116.7570	38	n/a	0	50	–	–	1.00	0	31.1496	0.5325	1155	1.318 ± 0.041	1.507 ± 0.047	–				
KF4	Qg3a	36.0610	116.7570	38	n/a	0	70	–	–	1.00	0	26.1512	0.4246	1155	0.913 ± 0.025	0.992 ± 0.027	–				
KF5	Qg3a	36.0610	116.7570	38	n/a	0	90	–	–	1.00	0	18.9587	0.4924	1155	0.729 ± 0.021	1.268 ± 0.037	–				
KF6	Qg3a	36.0610	116.7570	38	n/a	0	110	–	–	1.00	0	19.0129	0.5449	1155	0.913 ± 0.021	1.750 ± 0.040	–				
KF7	Qg3a	36.0610	116.7570	38	n/a	0	130	–	–	1.00	0	41.5864	0.5185	1155	1.813 ± 0.040	1.512 ± 0.034	–				
KF8	Qg3a	36.0610	116.7570	38	n/a	0	150	–	–	1.00	0	25.5572	0.5079	1155	1.177 ± 0.025	1.565 ± 0.037	–				

*Constant (time-invariant) local production rate based on Lal (1991) and Stone (2000). A sea-level, high-latitude value of 4.5 ± 0.3 atoms ^{10}Be g^{-1} quartz was used.
†Constant (time-invariant) local production rate based on Heisinger et al. (2002a, 2002b).
§A density of 2.7 g cm^{-3} was used for all surface samples.
#Isotope ratios were normalized to ^{10}Be standards prepared by Nishiizumi et al. (2007) with a value of 2.85 × 10^{-12} and using a 10Be half life of 1.36 × 10^6 years.
**Uncertainties are reported at the 1σ confidence level.
††A mean blank $^{10}Be/^{9}Be$ = 6.183 ± 0.833 × 10^{-15} was used to correct for background for samples beginning with KFMP. All other samples were corrected with a mean $^{10}Be/^{9}Be$ = 1.99 ± 0.48 × 10^{-15}.
§§Propagated uncertainties include error in the blank, carrier mass (1%), and counting statistics.
##Propagated error in the model ages include a 6% uncertainty in the production rate of ^{10}Be and a 4% uncertainty in the ^{10}Be decay constant.
***Beryllium-10 model ages were calculated with the CRONUS-Earth online calculator, version 2.2 (Balco et al., 2008; http://hess.ess.washington.edu/).

TABLE 2. SUMMARY OF OPTICALLY STIMULATED LUMINESCENCE (OSL) DATING RESULTS FROM EXTRACTED SEDIMENT, SAMPLE LOCATIONS, RADIOISOTOPE CONCENTRATIONS, MOISTURE CONTENTS, TOTAL DOSE RATES, D_E ESTIMATES, AND OPTICAL AGES

Sample number	Location (°N, °W)	Altitude (m below sea level)	Depth (cm)	Particle size (μm)	U* (ppm)	Th* (ppm)	K* (%)	Rb* (ppm)	Cosmic ray†,§ (Gy/k.y.)	Dose rate†,# (Gy/k.y.)	*n***	Mean equivalent dose†† (Gy)	OSL age§§ (ka)
Badwater													
KF4	36.226, 116.771	18	50	125–180	1.53	7.47	1.95	71.4	0.19 ± 0.02	2.59 ± 0.17	19 (54)	7.6 ± 0.6	2.9 ± 0.3
BWOSL9a	36.226, 116.771	26	200	125–180	1.61	7.91	2.56	75.6	0.16 ± 0.02	3.10 ± 0.21	33 (38)	15.7 ± 0.7	5.1 ± 0.4
BWOSL9b	36.226, 116.771	26	200	180-250	2.34	11.00	2.50	90.3	0.16 ± 0.02	3.03 ± 0.21	32 (38)	17.6 ± 1.3	5.8 ± 0.6
BWOSL10	36.226, 116.771	26	127	90–125	2.29	9.72	2.08	71.7	0.18 ± 0.02	3.08 ± 0.19	18 (27)	16.9 ± 0.8	5.5 ± 0.4
BWOSL11a	36.226, 116.771	26	56	125–180	1.61	7.91	2.56	75.6	0.19 ± 0.02	3.13 ± 0.22	17 (21)	10.0 ± 0.6	3.2 ± 0.3
BWOSL11b	36.226, 116.771	26	56	180–250	1.61	7.91	2.56	75.6	0.19 ± 0.02	3.06 ± 0.22	17 (40)	13.6 ± 1.4	4.4 ± 0.6
Mormon Point													
KF1a	36.061, 116.757	34	30	125–180	1.37	9.03	2.34	89.1	0.20 ± 0.02	2.98 ± 0.20	23 (33)	21.4 ± 1.0	7.2 ± 0.6
KF1b	36.061, 116.757	34	30	180–250	1.37	9.03	2.34	89.1	0.20 ± 0.02	2.92 ± 0.20	26 (30)	19.5 ± 1.0	6.7 ± 0.6
KF2	36.061, 116.757	34	38	125–180	1.50	9.33	2.54	96.2	0.20 ± 0.02	3.19 ± 0.22	18 (44)	24.7 ± 1.3	8.0 ± 0.7
MPOINT1	36.061, 116.757	38	110	125–250	1.47	9.23	3.58	106.0	0.18 ± 0.02	3.94 ± 0.29	24 (28)	28.1 ± 1.3##	7.8 ± 0.9
					1.97	12.10	2.57	99.8	0.18 ± 0.02	3.42 ± 0.23			
MPOINT2	36.062, 116.758	44	140	125–250	2.09	11.30	2.84	99.4	0.17 ± 0.02	3.61 ± 0.25	25 (28)	3.1 ± 0.4##	5.2 ± 0.8
					1.47	7.77	3.00	107.0	0.17 ± 0.02	3.39 ± 0.25			
MPOINT3	36.062, 116.758	44	135	125–180	2.03	12.00	2.83	98.0	0.18 ± 0.02	3.68 ± 0.25	27 (28)	14.7 ± 0.7##	4.1 ± 0.4
					2.20	10.70	2.61	102.0	0.18 ± 0.02	3.46 ± 0.23			

*Elemental concentrations from neutron activation analysis (NAA) of whole sediment measured at U.S. Geological Survey Nuclear Reactor Facility in Denver. Uncertainty taken as ±10%.

†Estimated fractional present-day water content for whole sediment is taken as 10% ± 5%.

§Estimated contribution to dose rate from cosmic rays calculated according to Prescott and Hutton (1988). Uncertainty taken as ±10%.

#Total dose rate from beta, gamma, and cosmic components. Beta attenuation factors for U, Th, and K compositions incorporating grain size factors from Mejdahl (1979). Beta attenuation factor for Rb is taken as 0.75 (cf. Adamiec and Aitken, 1998). Factors utilized to convert elemental concentrations to beta and gamma dose rates from Adamiec and Aitken (1998) and beta and gamma components attenuated for moisture content.

**Number of replicated equivalent dose (D_E) estimates used to calculate weighted mean D_E. These are based on recuperation error of <10%. The number in the parentheses is the total measurements made including failed runs with unusable data.

††Weighted mean equivalent dose (D_E) determined from replicated single-aliquot regenerative-dose (SAR; Murray and Wintle, 2000) runs. The uncertainty also includes an error from beta source estimate of ±5%.

§§Uncertainty incorporates all random and systematic errors, including dose rate errors and uncertainty for the D_E.

##Weighted mean of two dose rates from two sets of NAA were used to determine the age.

water visitor area (Fig. 4). These yielded ages ranging from 1.8 ± 0.4 ka to 14.2 ± 1.4 ka. The younger Qg3b deposits, both at the mouth of Bad Canyon and northeast of the visitor area, are ~1.5 m above the active channel and have relatively pale varnish colors (10R7/4).

The active channel deposits (Qg4a and Qg4b) have high-relief bar-and-swale topography. Although the Qg4a surface is elevated ~1 m above the active channel at the mouth of Bad Canyon, these channel deposits are latest Holocene in age, with unvarnished clasts and sharp bar-and-swale topography that is indistinguishable from the slightly younger Qg4b channels. Eight boulders (Badwater1 to Badwater8) were collected on the Qg4a deposit for ^{10}Be TCN dating. The samples yielded ^{10}Be exposure ages that range from 2.0 ± 0.5 ka to 73.4 ± 6.7 ka. We infer that these ages reflect inherited TCNs. The Qg4b deposits are mapped based on the fact that at the distal end, the Qg4b deposits overlie or erode the graded dirt road (Fig. 4) that was abandoned ca. 1940 according to Hunt and Mabey (1966). The exact year when the road was abandoned is not known. Hunt and Mabey (1966, p. 93) stated that the dirt road was abandoned "20–25 years ago." Whether Hunt and Mabey (1966) are referring to the publication year (1966) or the year field work began (1956) is unclear, so we use 1940 or 75 yr ago as a conservative estimate for when the road was abandoned. The fact that the dirt road is buried indicates that the Qg4b channel has been active in the past 75 yr—moving and rolling boulders during

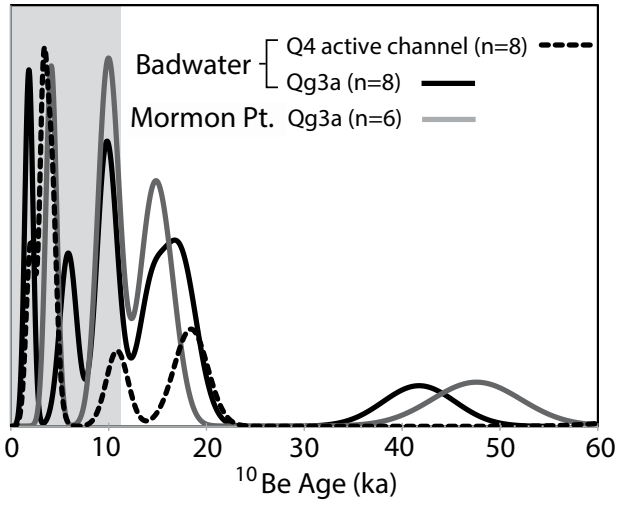

Figure 10. Probability distribution plots for ^{10}Be age on alluvial-fan surface at Badwater and Mormon Point. The gray area represents the Holocene.

TABLE 3. SUMMARY OF AGES FOR SURFACES AND SEDIMENTS FOR BADWATER AND MORMON POINT

Surface	TCN range (ka)	TCN average (ka)	Minimum upper OSL age (ka)	OSL age averaged for upper 2 m of sediment (ka)
Badwater				
Qg4a	2.0–71.0	16.5 ± 23.0	n/a	n/a
Qg3a	1.8–41.7	14.7 ± 12.2	2.9 ± 0.3	4.5 ± 1.2
Mormon Point				
Qg3a	4.1–47.6	16.9 ± 15.6	5.2 ± 0.8	7.0 ± 1.1

Note: TCN—terrestrial cosmogenic nuclide; OSL—optically stimulated luminescence.

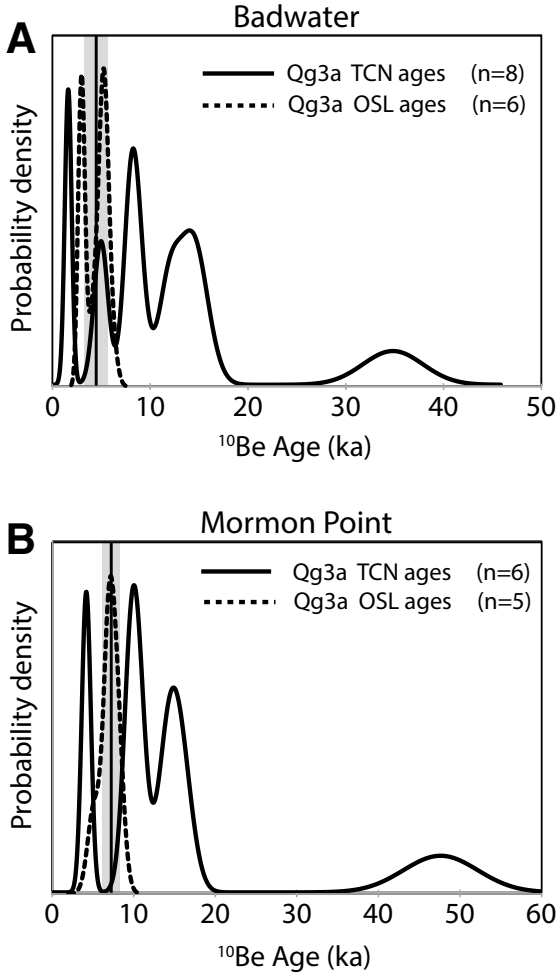

Figure 11. Probability distribution plots for ^{10}Be and optically stimulated luminescence (OSL) ages for Qg3a alluvial-fan sediments at (A) Badwater and (B) Mormon Point. The probability distribution function curves for the OSL ages represent the duration of sedimentation of the top 2 m of the fans, the average OSL is shown by the vertical red line, and the uncertainty (1σ) is shown by the pink bar. The colluvial wedge sample MPOINT3 is not included in the average OSL age. Average OSL ages are 7.0 ± 1.1 ka at Mormon Point and 4.5 ± 1.2 ka at Badwater.

that time. The Qg4b deposits are within the active channel and consist of unvarnished clasts with sharp bar-and-swale topography.

Badwater Faulting

The Black Mountains fault zone at Badwater varies from a single strand at the Bad Canyon alluvial fan apex to multiple, parallel strands northeast of the Badwater visitor area (Fig. 4). South of Bad Canyon, the Qg2b alluvial fan is offset vertically ~7 m across a single strand. Immediately north of the mouth of Bad Canyon, the Black Mountains fault zone splits into two strands that vertically offset the Qg3a alluvial fan a total of 6.4 ± 0.6 m (Fig. 6A). Northeast of the Bad Canyon alluvial fan, the Black Mountains fault zone is a single strand that separates the Quaternary alluvial fans and the Proterozoic bedrock. Northeast of the Badwater visitor area, the fault zone is expressed as six parallel fault scarps through the Qg3a and Qg3b alluvial-fan deposits (Fig. 4). All scarps northeast of the visitor area offset both the Qg3a and Qg3b alluvial fans ~2 m (Figs. 8A–8B). One scarp along the southern mountain front there, however, offsets a small post-Qg3b debris-flow fan along the mountain front on the southern margin, indicating the occurrence of at least two post-Qg3b surface ruptures.

A series of scarps offset the Qg3a deposits near the northwest margin of the Bad Canyon fan (Fig. 4). Although mapped as Qg3a/Qg4b, the scarps only offset the Qg3a alluvial fan surface, with the Qg4b channels eroded through the scarps. These scarps are nearly vertical and trend perpendicular to the fan gradient. Based on the orientation of the scarps and position near the salt playa, Wills (1989) interpreted these features as scarps formed by lateral ground spreading due to earthquake-induced liquefaction.

Mormon Point Stratigraphy

Six alluvial-fan deposits were mapped at Mormon Point (Fig. 5). The well-varnished, desert-pavement–mantled surface of the oldest alluvial-fan surface (Qg2a) is ~25 m above the active channel. The Qg2a surface is inset below the 120–186 ka Lake Manly deposits and was correlated by Knott et al. (2002) with the ca. 70 ka Qg2-equivalent deposits found elsewhere in Death Valley. The Qg2b deposit has darkly varnished clasts in a well-developed, but eroding, desert pavement surface that is ~5 m above the active channel.

Both the Qg3a and Qg3b alluvial fans have bar-and-swale topography. The bar-and-swale topography of the older Qg3a deposit has lower amplitude, and the clasts, especially carbonates, are weathered. The surface of the Qg3a deposit is ~2 m above the active channel. The Qg3b alluvial fan, which is inset ~0.5 m below the Qg3a deposit and ~1.5 m above the active channel, has strong bar-and-swale topography and moderately varnished clasts.

At Mormon Point, the probability density plots (Figs. 10–11) show peaks at ca. 4 ka, ca. 10 ka, ca. 15 ka, and ca. 48 ka for the ^{10}Be TCN surface ages from the Qg3a fan. The large spread of ages does not allow a conclusive interpretation of these data. In contrast, the five OSL ages from the Qg3a deposit yield a mean of 7.0 ± 1.1 ka, with little variation in depth within the fluvial fan deposits. A 7 ka age is consistent with the 4–8 ka age for the Qg3-equivalent alluvial fans in Death Valley estimated on the basis of soil development (e.g., Klinger and Piety, 2001). Machette et al. (2008) estimated the maximum age of the Qg3-equivalent deposits at 12–30 ka from ^{36}Cl depth profiling, and Sohn et al. (2014) used OSL to determine that the Qg3a age was 6–27 ka. Fundamentally, inheritance limits the interpretation of the TCN data; however, the 7.0 ± 1.1 ka OSL age is consistent with other age estimates and is our preferred age for the Qg3a deposit at Mormon Point.

The Qg4a deposits are colluvial, mainly forming off fault scarps. The Qg4a colluvial deposits are above the active channel and lack bar-and-swale topography, but they have generally unvarnished clasts. An OSL sample of the Qg4a deposit forming on a scarp offsetting the Qg3a deposit yielded an age of 4.1 ± 0.4 ka. The Qg4b deposits are within the active channels. The Qg4b deposit has bar-and-swale topography with relatively high relief and unvarnished clasts.

Mormon Point Faulting

The Holocene Black Mountains fault zone at Mormon Point exhibits a northern and southern strand (Fig. 5). These fault strands merge into a single strand to the east (within the mapped area) and west (outside the mapped area). The two strands at Mormon Point together vertically offset the Qg3a alluvial fan by 4.3 ± 0.6 m (Fig. 6A). The Qg3b surface, which is also displaced vertically by 4.3 ± 0.6 m, is the youngest offset alluvial-fan unit. Scarps on both strands have developing colluvial deposits (Qg4a) that are not faulted.

An impressive exposure through one of the normal faults at Mormon Point can be examined along the southern wall near the mouth of Ash Canyon (Fig. 12). Here, the normal fault is listric and displaces the upper Mormon Point Formation and the overlying 120–186 ka Lake Manly deposits (Lowenstein et al., 1999). In the hanging wall, the Lake Manly deposits dip more steeply than the upper Mormon Point Formation deposits, indicating syndepositional movement. The upper Mormon Point Formation contains the ca. 500 ka Dibekulewe ash bed just to the south outside the canyon (Knott et al., 1999).

DISCUSSION

Interpretation of Geochronological Data

The interpretation of excessive TCN ages (i.e., older than expected) as a consequence of surface processes or inheritance in alluvial environments is still debated (e.g., Behr et al., 2010). In this study, we show that alluvial-fan deposits that are less than 75 yr old have ^{10}Be TCN ages of 2–71 ka. If excess TCN were the result of in situ surface processes, then the boulders should yield TCN ages of ~75 yr or less. Our interpretation is that the 2–71 ka ages are the result of inherited TCN acquired during transport. As summarized in Machette et al. (2008), Holocene alluvium at several sites along the western side of Death Valley has inherited ^{36}Cl TCN equivalent to 46–94 ka. Our study reaffirms that TCN methods are not easily applied to date Holocene alluvial-fan surfaces in environments throughout Death Valley, and likely in most other similar settings, because inherited TCNs overwhelm the concentrations acquired in depth profiles and surface clasts. This may be the case for other, similar depositional settings, and care should be taken when planning campaigns for dating late Holocene tectonic landforms in such environments.

Similarly complex variations in ^{10}Be TCN ages for lower Holocene deposits suggestive of complicated inheritance have been observed in other studies in Death Valley. For example, Frankel et al. (2007a, 2007b), Machette et al. (2008), and Owen et al. (2011) all found that inheritance was significant for boulders on early Holocene to late Pleistocene landforms in Death Valley. In this study, we used probability density functions in combination with another dating method within a reasonably well-established stratigraphic framework to attempt an interpretation of the TCN dating. Even with the insight provided by previous studies and independent geochronologic data, the TCN ages are ambiguous. Presenting these data is particularly important for helping to guide future research in this and similar environments.

In contrast, OSL methods produced consistent ages of deposition within the local stratigraphic framework. The progressively older OSL ages with depth and the stratigraphically correct ages on the alluvial-fan deposit and the unfaulted colluvium are evidence of consistent results from OSL.

An alternate interpretation of the OSL ages at Badwater is that the 5.1–5.8 ka ages at depth represent the depositional age, and the shallower OSL ages are younger due to eluviation of fine particles. OSL ages obtained from highly permeable Lake Manly deposits showed similarly "too young" ages that Owen et al. (2011) hypothesized were due to eluviation. At Badwater, the debris-flow deposits may allow eluviation of fines; however, we did not observe clay films or other features that are indicative of translocating clays and silts.

Black Mountains Fault Zone Earthquakes: Timing of Ground-Rupturing Earthquakes

True paleoseismologic data are sparse from the Black Mountains fault zone, and indeed from the entire Death Valley fault zone, because of National Park Service restrictions on excavations and the lack of datable carbon in the alluvial deposits along the fault. Thus, the earthquake history of this major fault system remains poorly defined. Nevertheless, previous workers have used detailed geomorphic analysis as well as luminescence dating to shed some light on previous earthquake occurrence. Most basically, analysis of scarp profiles reveals beveling of the scarps suggestive of periods of punctuated scarp development and subsequent modification (Frankel et al., 2001; Klinger and Piety, 2001; Machette and Crone, 2001; Sohn et al., 2014). These analyses indicate the occurrence of several Holocene earthquakes along the Black Mountains fault zone and suggest a potentially complicated space-time pattern of earthquakes (Machette et al., 2001), possibly reflecting significant structural segmentation of the fault at seismogenic depths.

For example, along the southernmost part of the Black Mountains fault zone (section 1), Sohn et al. (2014) used OSL dating and fault-scarp morphology to show that two, and likely three, ground-rupturing earthquakes have displaced a Qg3b alluvial fan in the last 4–9 k.y. East of Mormon Point, Klinger and Piety (2001) found evidence of four ground-rupturing earthquakes in the fault scarps offsetting the 4–8 ka Qg3b alluvial fan; however, pedogenesis may help strengthen the fanglomerates so that they do not erode easily, leading to oversteepening of parts of the scarps that could complicate their interpretation.

The OSL sample collected from the colluvial wedge at Mormon Point yielded an age of 4.1 ± 0.4 ka (Fig. 9B) for the colluvium deposited across

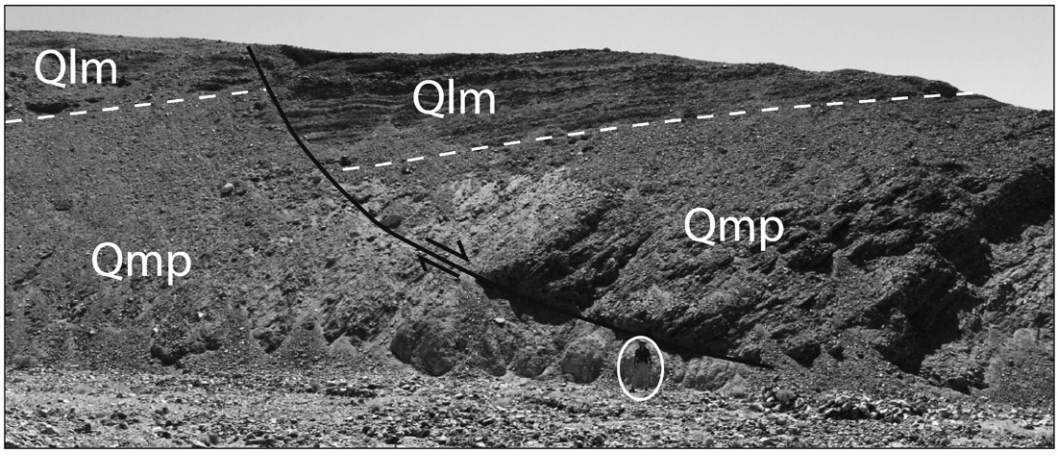

Figure 12. View looking south at a low-angled normal fault at Ash Canyon (36.0548°N, 116.7637°W). Note person for scale. Qlm—Lake Manly deposits, ca. 120–186 ka; Qmp—Mormon Point Formation, ca. 550 ka.

the scarp of this ground-rupturing earthquake. Given the mode of development of the colluvial wedge (initial collapse of the fault scarp and subsequent erosion and deposition), this OSL age could reflect a mixture of grains that were well-zeroed during deposition and other grains that may not have been well zeroed, resulting in an apparently older age for the deposit. Thus, we consider this age to be a maximum for the most recent surface-rupturing earthquake at Mormon Point. The colluvial wedge is younger than the 7 ka age of the Qg3a deposit, which has been faulted by at least one surface rupture. Because the fault strands merge to the east and west and offset the same deposits, it is not possible to determine if the Mormon Point scarps record a single earthquake on a splaying fault or two separate earthquakes. The ≤4 ka age of the colluvial wedge is either at the youngest end of, or is younger than, the 4–8 ka range of the soil-based age estimates for a ground-rupturing event along this section of the Black Mountains fault zone (Klinger and Piety, 2001). We emphasize, however, that the colluvial wedge OSL age may be older than the true initial depositional age of the colluvial deposit, suggesting that the most-recent event at Mormon Point may be younger than 4 ka.

The morphology of the Black Mountains fault zone at Badwater is similar to that of Mormon Point in that the fault anastomoses into two strands north of the mouth of Bad Canyon. Further north, east of the Badwater visitor area, the Black Mountains fault zone is a single strand, but then it anastomoses again into multiple fault strands to the northeast. Along most of the trend, the Black Mountains fault zone offsets both the 4.5 ka Qg3a and the younger Qg3b alluvial units; however, northeast of the visitor area, one strand of the fault offsets a debris cone that overlies Qg3b, whereas the other fault strands do not. These crosscutting relations indicate the occurrence of at least two ground-rupturing earthquakes across the alluvial fan northeast of Badwater since deposition of the Qg3a deposit ca. 4.5 ka.

Currently available paleoseismic age constraints are not precise enough to determine if sections 1 through 4 of the Black Mountains fault zone all ruptured together in separate post-Qg3a and subsequent post-Qg3b earthquakes that encompassed the entire southern two thirds of the fault, or if the scarps observed on sections 1, 3, and 4 were the product of isolated earthquakes that ruptured each section. Crosscutting relations on southernmost section 1 (Sohn et al., 2014) and the north-central section 4 at Badwater (this study) indicate the occurrence of at least two ground-rupturing earthquakes on the Black Mountains fault zone in the last 4.5–9 k.y., with the likely occurrence of at least three separate events along the southernmost part of the Black Mountains fault zone. The liquefaction-induced lateral spreading near Badwater (Wills, 1989) occurred after 4.5 ka and may or may not have been coincident with the formation of the fan apex fault scarps.

These geomorphic observations leave open the possibility that the 6.4-m-tall scarp that we measured at Badwater could have formed in a single earthquake. We suggest, however, that it is likely that the Badwater scarp was generated by at least two surface ruptures, rather than a single event. Our reasoning is twofold: First, offset of a post-Qg3b debris cone suggests that at least two surface ruptures have occurred in this area since deposition of the Qg3a fan surface, which is dated at ≤4.5 ka. Second, rupture of the entire 60-km-long Black Mountains fault zone, with a downdip fault width of 14–15 km, based on 13 km seismogenic depth and 60°–70° fault dips, would generate a rupture of ~840–900 km^2, commensurate with the range of magnitudes from Wells and Coppersmith's (1994) global regressions of rupture area with moment magnitude of ~M_w 7.0. Average displacements of such events are typically on the order of 1–2 m (Wells and Coppersmith, 1994). In contrast, the ~7 m of dip-slip fault displacement that would be required to generate the 6.4-m-tall Badwater scarp would typically be generated by much larger-magnitude earthquakes. Specifically, an average displacement of 7 m is typical of M_w ~7.7 earthquakes (Wells and Coppersmith, 1994). Earthquakes of this size typically involve rupture areas on the scale of ~4000–5000 km^2. Although it would be possible to generate a rupture of this size involving solely the Black Mountains fault zone through Badwater, such an earthquake likely would require rupture of the entire 250-km-long northern Death Valley fault zone, which seems unlikely to us in light of the numerous along-strike complexities in this system. Our preferred interpretation is therefore that the scarp at Badwater records multiple surface-rupturing earthquakes, and thus we can use this displacement to reasonably infer the mid–late Holocene slip rate of the Black Mountains fault zone spanning multiple earthquake cycles.

Fault Slip Rates and Horizontal Extension Rates

Vertical Component of Fault Slip Rates

We used the measured scarp heights and our OSL ages to calculate the vertical component of fault slip rates at Badwater and Mormon Point. To constrain the resulting range of the vertical-component rates, we used the method of Zechar and Frankel (2009; see also Kozacı et al., 2009), which takes a probabilistic approach to calculate uncertainty. Displacements, ages, and slip rates are treated as probability density functions, and uncertainties of each measurement are propagated through the calculation. The vertical displacement combined with the exposure age yielded the vertical component of the overall fault slip rate.

Combining the vertical component of overall fault displacement of 6.4 ± 0.6 m with the exposure age of 4.5 ± 1.2 ka for the Qg3a surface of the Badwater fan yields a vertical component of the fault slip rate of 1.4 +0.5/–0.3 mm/yr (1σ uncertainty about the median; Fig. 13; Table 4). At Mormon Point, the combination of the vertical component of displacement of the Qg3a alluvial-fan surface of 4.3 ± 0.6 m with the exposure age of 7.0 ± 1.1 ka yields a vertical component of the slip rate of 0.6 ± 0.1 mm/yr (1σ uncertainty about the median).

Normal Fault Slip Rates

Conversion of the vertical component of the overall fault slip into true normal fault dip-slip rates depends on the Black Mountains fault zone dip. The dip of the Black Mountains fault zone dip, however, is variable and difficult to measure. There are, however, estimates of local fault dip at both Badwater and Mormon Point that we can use to refine these rates. Specifically, the Black Mountains fault zone at Badwater separates basement rock from basin deposits (Fig. 4) and is the steeply dipping limb of the Badwater turtleback fault (Miller, 1991; Blakely et al., 1999). Based on gravity and magnetic data, Hunt and Mabey (1966) showed that the eastern margin of Death Valley at Badwater dips more steeply than the western margin. Miller (1991) measured the Badwater turtleback fault dipping 42°–52° at Badwater. Hayman et al. (2003) showed that the strike of the high-angle, hanging-wall faults, including the Holocene Black Mountains fault zone, is dependent on the orientation of the W-dipping Badwater turtleback fault, and, where exposed, the high-angle faults sole into, but do not offset, the basin-bounding Badwater turtleback fault. In the subsurface, gravity data interpreted by Blakely et al. (1999) showed that, at depth, the Black Mountains fault zone dips ~60°–70° at Badwater. Based on the geophysical and outcrop data, we assume a 60°–70° dip at Badwater for the Black Mountains fault zone. Combining the vertical component of slip with the fan ages and fault dips discussed here allows us to estimate the dip-slip normal fault slip rate of the Black Mountains fault zone. At Badwater, the 60°–70° dip of the fault and the vertical rate of 1.4 +0.5/–0.3 mm/yr yield a dip-slip rate of 1.6 +0.6/–0.4 mm/yr.

The fault geometry at Mormon Point may also be inferred from outcrop data (e.g., Ash Canyon, Fig. 12), and geophysical models. The gravity model by Hunt and Mabey (1966) suggests a more gentle fault dip north

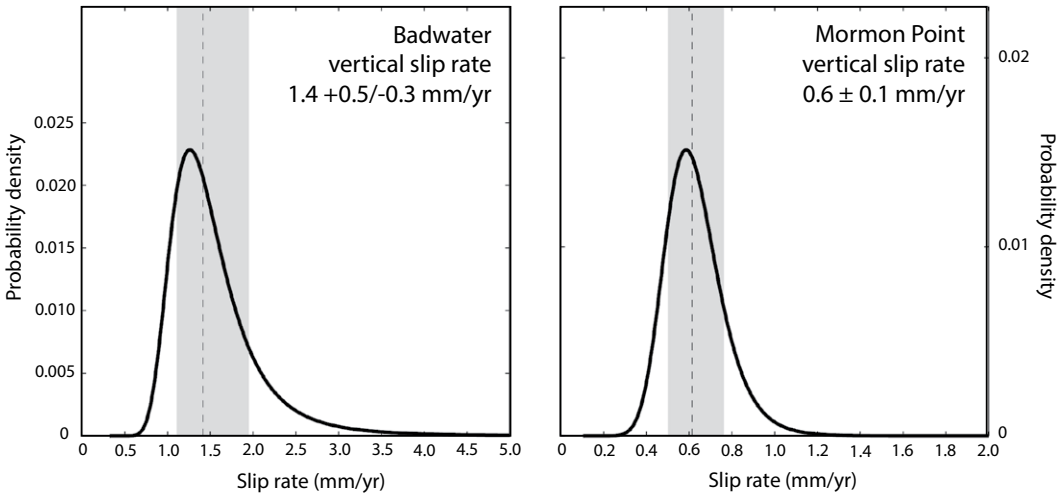

Figure 13. Probability distribution functions for vertical displacement rates for Qg3a surfaces at Badwater and Mormon Point.

TABLE 4. ALLUVIAL-FAN DISPLACEMENTS, AGES, AND SLIP RATES ALONG THE BLACK MOUNTAIN FAULT ZONE

Alluvial-fan deposit	Vertical offset (m)	Age (ka)	Vertical slip rate (mm/yr)	Favored fault dip (°)	Horizontal slip rate (mm/yr)			Fault-perpendicular extension direction (°)	Slip rate toward 323° for 60°-dipping fault (mm/yr)*	Slip rate toward 323° for 30°-dipping fault (mm/yr)*
					Dip = 30°	Dip = 70°	Dip = 60°			
Badwater	6.4 ± 0.6	4.5 ± 1.2	1.4 +0.5/–0.3	60	2.4 +0.9/–0.5	0.5 +0.2/–0.1	0.8 +0.3/–0.2†	322	0.8 +0.3/–0.2†	2.4 +0.9/–0.5
Mormon Point	4.3 ± 0.6	7.0 ± 1.1	0.6 ± 0.1	30	1.0 ± 0.2†	0.2 ± 0.1	0.3 ± 0.1	343	0.3 ± 0.2	1.0 ± 0.2†

*Horizontal slip rate projected parallel to Pacific–North America plate motion (Dixon et al., 2000).
†Preferred fault dip.

of Mormon Point, where our study is located, and a more steeply dipping fault to the west. Keener et al. (1993) reached a similar conclusion using gravity and magnetic data. Keener et al. (1993) showed in their model that the Holocene Black Mountains fault zone dipped ~70°NW and offset the low-angle (30° dip) Mormon Point turtleback fault (Fig. 5A). In contrast, Hayman et al. (2003) measured strikes and dips of high-angle and low-angle faults at Mormon Point and determined that the orientation of the high-angle faults, like the Holocene Black Mountains fault zone at our study site, is controlled by the 30°NW-dipping Mormon Point turtleback fault. Where the high-angle and low-angle faults were exposed, the high-angle faults soled into the low-angle fault and did not offset the low-angle fault. Thus, Hayman et al. (2003) concluded that the 30°NW-dipping Mormon Point turtleback fault was the seismogenic fault, and the Holocene Black Mountains fault zone soled into that fault. In addition, where depth of exposure is sufficient, the Quaternary faults show listric geometries (Fig. 12); thus, the steeply dipping, scarp-forming fault we observed at the surface likely has a low-angle dip at depth. Based on the fault geometry inferred by Hayman et al. (2003) and the outcrop data, we assume that the seismogenic fault that formed the Holocene scarp at Mormon Point dips at 30°NW. Combining the inferred 30° dip of the fault and the vertical rate of 0.6 ± 0.1 mm/yr yields a dip-slip rate of 1.2 +0.3/–0.2 mm/yr, i.e., slightly slower than the 1.6 +0.6/–0.4 mm/yr rate at Badwater.

Horizontal Extension Rates

As with determination of the fault dip-slip rates, converting the measured vertical component of the overall fault slip into fault-perpendicular horizontal extension rates depends on the Black Mountains fault zone dip. Assuming a range of possible fault dips from 30° to 70°, we trigonometrically determined a range of fault-strike–perpendicular horizontal extension rates from 2.4 +0.9/–0.5 mm/yr (30° dip) to 0.5 +0.2/–0.1 mm/yr (70° fault dip) for Badwater. If we assume a fault dip for the Black Mountains normal fault at Badwater of 60°–70°, consistent with fault dips observed in outcrop and in geophysical data (Blakely et al., 1999) and as predicted by classical theory (Anderson, 1951), this yields a horizontal extension rate of 0.5 +0.2/–0.1 mm/yr to 0.8 +0.3/-0.2 mm/yr directed toward 322° (i.e., N38°W; Fig. 6B; Table 4).

At Mormon Point, the preferred 30° dip of the Black Mountains fault zone yields a fault-perpendicular horizontal extension rate of 1.0 ± 0.2 mm/yr directed toward 343° (i.e., N17°W). Projecting these extension rates toward 323°, parallel to Pacific–North America plate motion of Dixon et al. (2000), yields rates of 0.5 +0.2/–0.1 mm/yr (70° fault dip) to 0.8 +0.3/–0.2 mm/yr (preferred 60° fault dip) at Badwater and 1.0 ± 0.2 mm/yr at Mormon Point.

The extension rates we determined are similar to the 1–3 mm/yr slip rate estimated by Klinger and Piety (2001) on section 3 of the Black Mountains fault zone at Mormon Point; however, they used a soil-based 4–8 ka age for the displaced surface and assumed a vertical fault. Knott and Wells (2001) determined a minimum slip rate of 0.2 mm/yr for section 3 of the Black Mountains fault zone south of Badwater. Sohn et al. (2014), who also assumed a vertical fault, determined a horizontal rate of 0.2–1.8 mm/yr on section 1 south of Mormon Point. Thus, the Holocene rates produced in this study are consistent with the limited data available along the Black Mountains fault zone.

Our Holocene extension rates for Badwater and Mormon Point are shown on Figure 14 together with the slip and extension rates for the Eastern California shear zone compiled by Ganev et al. (2010). The 0.5 +0.2/–0.1 mm/yr to 0.8 +0.3/–0.2 mm/yr Holocene extension rate at Badwater for a 60°–70°-dipping fault is toward the upper limit for extension rates on

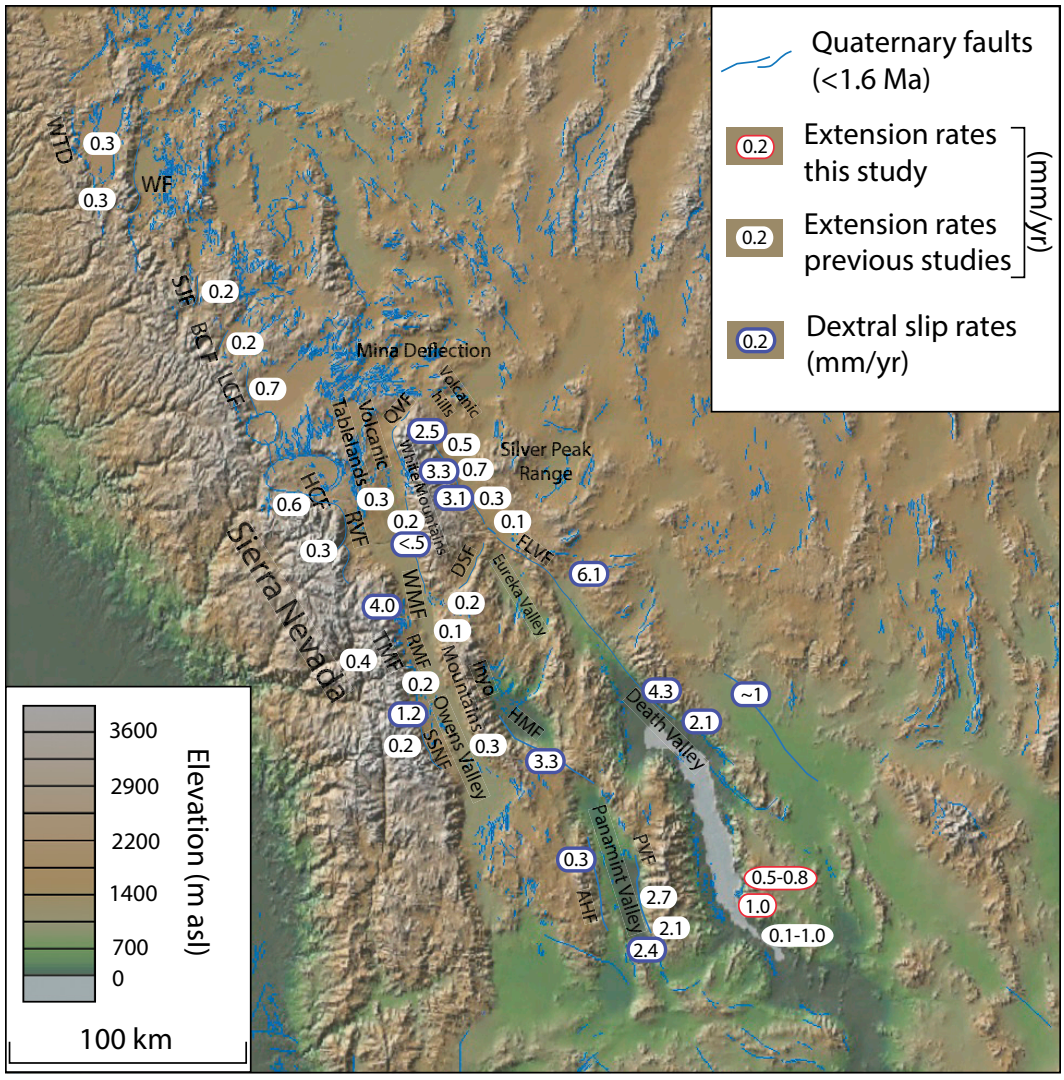

Figure 14. Digital elevation model produced using GeoMapApp (http://www.geomapapp.org/; asl—above sea level), showing the major Quaternary faults (younger than 1.6 Ma) taken from U.S. Geological Survey (USGS, 2014) showing extension rates (mm/yr). The extension rate values presented in Ganev et al. (2010), who resolved the extension rates by assuming a 60° fault dip on the faults in publications where the authors reported only the vertical component of slip, are used. Primary data for the rates on the Round Valley fault (RVF) and Hilton Creek fault (HCF) are from Berry (1997), the rate on the Volcanic Tablelands is from Sheehan (2007), and the rate on the White Mountains fault (WMF) is from Kirby et al. (2006). The rates on the Fish Lake Valley fault are from Ganev et al. (2010), and those from Panamint Valley are from Hoffman (2009). Extension rates for the Lundy Canyon, Buckeye Creek, and Sonora Junction faults and West Fork Carson River fault at Woodfords are from Rood et al. (2011). Rates of dextral slip on strike-slip faults were taken from Frankel et al. (2011), with primary data from Zhang et al. (1990), Densmore and Anderson (1997), Lee et al. (2001b, 2009), Oswald and Wesnousky (2002), Kirby et al. (2006), Guest et al. (2007), Frankel et al. (2007a, 2007b, 2011), and Ganev et al. (2010). Rates south of Mormon Point in Death Valley are from Sohn et al. (2014). DSF—Deep Springs fault, FLVF—Fish Lake Valley fault, HCF—Hill Creek fault, QVF—Queen Valley fault, RVF—Round Valley fault, LCF—Lundy Canyon, BCF—Buckeye Creek, SJF—Sonora Junction, WF—Woodfords, WTD—West Tahoe–Dollar Point fault, HMF—Hunter Mountain fault, AHF—Ash Hill fault, PVF—Panamint Valley fault, TMF—Tinemaha Creek frontal fault, SSNF—Southern Sierra Nevada frontal fault zone, RMF—Red Mountain fault.

faults in the western Basin and Range. If the seismogenic fault at Mormon Point is the 30°-dipping fault, then the extension rate at Mormon Point is 1.0 ± 0.2 mm/yr. These data suggest that the Black Mountains fault zone accommodates a large component of Basin and Range extension at this latitude, although the Death Valley extension rates detailed here are considerably slower than ~2–2.5 mm/yr extension rates reported from the same latitude on the Panamint Valley fault to the west (Hoffman, 2009).

Regional Implications: Comparison of Central Death Valley Rates with Rates on Nearby Faults

Our Holocene extension rates for Badwater and Mormon Point are shown on Figure 14 together with the slip and extension rates for the Eastern California shear zone compiled by Ganev et al. (2010). Interestingly, the NNW-directed horizontal rates we measured at Badwater and Mormon Point are slower than the 2.1 +0.5/–0.4 mm/yr rate measured by Frankel et al. (2011) along the southern part of the dextral northern Death Valley fault system north of the Black Mountains fault zone. It is worth noting, however, that the faults we studied at Badwater and Mormon Point are associated with hanging-wall strands of the Black Mountains fault zone that probably sole downward into the master Black Mountains turtleback fault at depth, and they likely have relatively small cumulative displacements. This suggests that slip along these strands may be less localized than it would be along more structurally mature fault strands (e.g., Dolan and Haravitch, 2014). Thus, the apparent discrepancy between the Black Mountains fault zone rates we measured and the southern northern Death Valley fault zone rate at South Mud Canyon may be somewhat smaller than it appears. Nevertheless, even with the likelihood of less-focused slip on the Badwater and Mormon Point hanging-wall strands in mind, the NNW-directed Black Mountains fault zone extension rates we measured in central Death Valley are still likely slower than the rate of the southern part of the northern Death Valley fault zone to the north. This southward decrease in NNW-directed horizontal extension rates from the southern Death Valley fault zone to the Black Mountains fault zone in central Death

Valley is part of a more general observation of southward-decreasing rates measured on the northern Death Valley fault system south of Cucomongo Canyon in northernmost Death Valley (Fig. 1; Frankel et al., 2011).

The Black Mountains fault zone horizontal rates are only about half as fast as NNW-oriented horizontal rates documented in previous studies in southern Panamint Valley to the west of Death Valley. Specifically, Hoffman (2009) determined NNW-directed horizontal rates of 2.1 ± 0.5 mm/yr at Manly Peak Canyon and 2.7 ± 1.5 mm/yr at Happy Canyon farther north along the Panamint Valley fault zone at approximately the latitude of our rates in central Death Valley (Fig. 1). These observations, which suggest that additional strain may be transferred southwestward from the northern Death Valley fault zone and northern end of the Black Mountains fault zone onto the oblique-normal dextral faults of the Panamint Valley fault zone, are consistent with geodetic block-model results that suggest that current opening rates of Panamint Valley are approximately three times faster than opening rates of central Death Valley (Meade and Hager, 2005). As noted in previous studies (Reheis and Dixon, 1996; Klinger and Sarna-Wojcicki, 2001; Lee et al., 2001a; Knott et al., 2005; Frankel et al., 2011), much of this slip transfer between the northern Death Valley fault zone system and the Panamint Valley fault zone in southern and central Panamint Valley probably occurs along the Towne Pass and related faults to the north of the Black Mountains fault zone (Fig. 1). However, the slower NNW-directed horizontal rates that we measured along the Black Mountains fault zone in central Death Valley relative to the southern northern Death Valley fault zone indicate that additional slip is transferred off the Death Valley fault system. Two possible hypotheses that explain the slip deficit between the northern Death Valley fault zone and Black Mountains fault zone are: slip is transferred to the Panamint Valley fault zone on distributed faults south of the Towne Pass fault (Cowan and Bodin, 2014), or slip is accommodated by the Quaternary faults on west side of Death Valley (Hunt and Mabey, 1966; Brogan et al., 1991).

Adding the slip rates of the two most prominent faults in the northern part of the Eastern California shear zone at the latitude of central Death Valley—the Black Mountains fault zone and Panamint Valley fault zone—yields a cumulative NNW-directed horizontal rate of ~3.0–3.5 mm/yr. This is only approximately one quarter to one third of the total ~9–12 mm/yr rate of shear across this region indicated by modeling of the geodetic velocity field (e.g., Bennett et al., 2003; Meade and Hager, 2005). Although some of the remainder of this "missing" slip is accommodated by other known faults, such as the Ash Hill fault (Densmore and Anderson, 1997) and the wide zone of faulting extending southward from the southern end of the Owens Valley fault in the Coso region, these faults are all very slow slip rate structures, and the cumulative total across this entire zone is probably only 1 mm/yr or so (e.g., Le et al., 2007; Frankel et al., 2008, and references therein; Rood et al., 2011). Thus, slip on known faults at the latitude of central Death Valley likely only accounts for part—likely no more than half—of the total NNW dextral shear across this region. Distributed processes must accommodate the remainder. This observation highlights the fact that along many parts of the northern Eastern California shear zone north of the Garlock fault, much of the total slip is not accommodated on major faults (Frankel et al., 2011).

CONCLUSIONS

Our study stresses the limitations and challenges of applying ^{10}Be TCN methods to date Holocene geomorphic surfaces in Death Valley and similar settings where sediment flux is slow and complex. However, OSL dating produced surface ages consistent with the regional stratigraphy. At Badwater, we determine an OSL age of 4.5 ± 1.2 ka and a ^{10}Be TCN age of 9–43 ka for the faulted Qg3a alluvial fan. At Mormon Point, the ages for the faulted Qg3a alluvial fan are 7.0 ± 1.0 ka and 4–48 ka by OSL and ^{10}Be TCN, respectively. The clasts in the active channel (Qg4a and Qg4b), deposited in the past 75 yr in some cases, yield ^{10}Be TCN ages of 2–71 ka, attesting to significant and complicated patterns of inheritance.

The OSL ages of 4.5 ± 1.2 ka at Badwater and 7.0 ± 1.0 ka at Mormon Point on the faulted Qg3a alluvial-fan surfaces, however, provide reasonable surface ages within the known geomorphic and stratigraphic framework, albeit with relatively large uncertainties. Using our OSL data, the vertical components of fault slip rates for the Badwater and Mormon Point Qg3a alluvial-fan surfaces are 1.4 +0.5/–0.3 mm/yr and 0.6 ± 0.1 mm/yr, respectively. Available outcrop and geophysical data indicate that the seismogenic faults at Mormon Point and Badwater dip at 30° and at 60°–70°, respectively. These observations, combined with the uplift rate we measured, yield dip-slip rates of 1.2 +0.3/–0.2 mm/yr at Mormon Point and 1.6 +0.6/–0.4 mm/yr at Badwater, and horizontal extension rates of 1.0 ± 0.2 mm/yr along 343° at Mormon Point and 0.5+0.2/–0.1 to 0.8 +0.3/–0.2 mm/yr along 322° at Badwater. These NNW horizontal rates are somewhat slower than the ~2 mm/yr dextral slip rate of the southern end of the NNW-trending northern Death Valley fault zone extending northwards from the Black Mountains fault zone. Moreover, the Black Mountains fault zone horizontal rates are less than half as fast as NNW-oriented horizontal rates documented in previous studies in southern Panamint Valley to the west of Death Valley. These observations, which indicate that additional strain is transferred southwestward from the northern Death Valley fault zone and northern end of the Black Mountains fault zone onto the oblique-normal dextral faults of the Panamint valley fault zone, are consistent with published geodetic modeling showing that current opening rates of central Death Valley along the Black Mountains fault zone are about three times slower than opening rates in Panamint Valley. Moreover, addition of these slip rates, together with published slip rates from faults within the transition zone between the Eastern California shear zone and Basin and Range Province to the west of Death Valley, suggest that less than about one half of the geodetically determined ~9–12 mm/yr of right-lateral shear across the region at the latitude of central Death Valley is accommodated by slip on well-defined faults. We suggest that distributed deformational processes take up the remainder of this slip, partly as slip is transferred between the major faults of the region north of the Garlock fault.

The OSL dating also provides an age of 4.1 ± 0.4 ka from the basal colluvial wedge forming off a scarp cutting the 7.0 ± 1.0 ka alluvial fan at Mormon Point, defining a maximum age of the most-recent earthquake along the Black Mountains normal fault zone in central Death Valley. Coupled with published geomorphic observations, this age suggests a potentially complicated space-time pattern of earthquake occurrence along the Black Mountains fault zone.

ACKNOWLEDGMENTS

This study was supported by National Science Foundation grants EAR-0537901 and EAR-0537580, with additional support from a NASA Earth System Science Fellowship, the Georgia Institute of Technology, the University of Southern California Department of Earth Sciences Student Research Fund, California State University–Fullerton Department of Geological Sciences, and the University of California White Mountain Research Station. Stephanie Briggs, Jeremy Zechar, and Jeremy Hatfield are thanked for their assistance with field work, and Alicia Nobles is thanked for her help with sample preparation. Sincere thanks go to editor Kurt Stüwe, reviewer Terry Pavlis, and an anonymous reviewer for their very constructive and useful comments in helping us improve our manuscript. This manuscript is Open Access in honor of the memory of Kurt Frankel. Kurt is greatly missed by all his family, friends, and academic community.

REFERENCES CITED

Adamiec, G., Aitken, M., 1998, Dose rate conversion factors: update: Ancient TL, v. 16, p. 37–49.
Anderson, E.M., 1951, The Dynamics of Faulting: London, Oliver and Boyd, 206 p.
Anderson, R.S., Repka, J.L., and Dick, G.S., 1996, Dating depositional surfaces using in situ produced cosmogenic radionuclides: Geology, v. 24, p. 47–51, doi:10.1130/0091-7613(1996)024<0047:ETOIID>2.3.CO;2.

Balco, G., Stone, J.O., Lifton, N.A., and Dunai, T.J., 2008, A complete and easily accessible means of calculating surface exposure ages or erosion rates from ^{10}Be and ^{26}Al measurements: Quaternary Geochronology, v. 3, p. 174–195, doi:10.1016/j.quageo.2007.12.001.

Behr, W.M., Rood, D.H., Fletcher, K.E., Guzman, N., Finkel, R.C., Hanks, T.C., Hudnut, K.W., Kendrick, K.J., Platt, J.P., Sharp, W.D., Weldon, R.J., II, and Yule, J.D., 2010, Uncertainties in slip-rate estimates for the Mission Creek strand of the southern San Andreas fault at Biskra Palms Oasis, southern California: Geological Society of America Bulletin, v. 122, no. 9–10, p. 1360–1377, doi:10.1130/B30020.1.

Bennett, R.A., Wernicke, B.P., Niemi, N.A., Friedrich, A.M., and Davis, J.L., 2003, Contemporary strain rates in the northern Basin and Range Province from GPS data: Tectonics, v. 22, p. 1008, doi:10.1029/2001TC001355.

Berry, M.E., 1997, Geomorphic analysis of late Quaternary faulting on Hilton Creek, Round Valley and Coyote Warp faults, east-central Sierra Nevada, California, USA: Geomorphology, v. 20, p. 177–195, doi:10.1016/S0169-555X(97)00033-0.

Blakely, R.J., Jachens, R.C., Calzia, J.P., and Langenheim, V.E., 1999, Cenozoic basins of the Death Valley extended terrane as reflected in regional-scale gravity anomalies, *in* Wright, L.A., and Troxel, B., eds., Cenozoic Basins of the Death Valley Region: Geological Society of America Special Paper 333, p. 1–16, doi:10.1130/0-8137-2333-7.1.

Brogan, G.E., Kellogg, K.S., Slemmons, D.B., and Terhune, C.L., 1991, Late Quaternary Faulting Along the Death Valley–Furnace Creek Fault System, California and Nevada: U.S. Geological Survey Bulletin 1991, p. 1–23.

Budahn, J.R., and Wandless, G.A., 2002, Instrumental Neutron Activation by Abbreviated Count: U.S. Geological Survey Open-File Report 02-223, online only at http://pubs.usgs.gov/of/2002/ofr-02-0223/ (last accessed 9 September 2015).

Bull, W.B., 1968, Alluvial-fans: Journal of Geological Education, v. 16, p. 101–106.

Bull, W.B., 1991, Geomorphic Responses to Climate Change: New York, Oxford University Press, 326 p.

Burchfiel, B.C., and Stewart, J.C., 1966, "Pull-apart" origin of the central segment of Death Valley, California: Geological Society of America Bulletin, v. 77, p. 439–442, doi:10.1130/0016-7606(1966)77[439:POOTCS]2.0.CO;2.

Butler, P.R., Troxel, B.W., and Verosub, K.L., 1988, Late Cenozoic history and styles of deformation along the southern Death Valley fault zone, California: Geological Society of America Bulletin, v. 100, p. 402–410, doi:10.1130/0016-7606(1988)100<0402:LCHASO>2.3.CO;2.

Cowan, D.S., and Bodin, P., 2014, Searching for microearthquakes on detachment faults beneath Death Valley, California: Geological Society of America Abstracts with Programs, v. 46, no. 5, p. 23.

DeMets, C., and Dixon, T.H., 1999, New kinematic models for Pacific–North America motion from 3 Ma to present: I. Evidence for steady motion and biases in the NUVEL-1A model: Geophysical Research Letters, v. 26, no. 13, p. 1921–1924, doi:10.1029/1999GL900405.

Denny, C.S., 1965, Alluvial Fans in the Death Valley Region, California and Nevada: U.S. Geological Survey Professional Paper 466, 62 p., with 5 plates.

Densmore, A.L., and Anderson, R.S., 1997, Tectonic geomorphology of the Ash Hill fault, Panamint Valley, California: Basin Research, v. 9, p. 53–63, doi:10.1046/j.1365-2117.1997.00028.x.

Desilets, D., Zreda, M., Prabu, T., 2006, Extended scaling factors for in situ cosmogenic nuclides: new measurements at low latitude: Earth and Planetary Science Letters, v. 246, p. 265–276.

Dixon, T., Robaudo, S., Lee, J., and Reheis, M.C., 1995, Constraints on present-day Basin and Range deformation from space geodesy: Tectonics, v. 14, no. 4, p. 755–772, doi:10.1029/95TC00931.

Dixon, T., Farina, F., DeMets, C., and Suarez Vidal, F., 2000, New kinematic models for Pacific–North America motion from 3 Ma to present: II. Evidence for a "Baja California shear zone": Geophysical Research Letters, v. 27, no. 23, p. 3961–3964, doi:10.1029/2000GL008529.

Dolan, J.F., and Haravitch, B.D., 2014, How well do surface slip measurements track slip at depth in large strike-slip earthquakes? The importance of structural maturity in controlling on-fault versus off-fault deformation: Earth and Planetary Science Letters, v. 388, p. 38–47, doi:10.1016/j.epsl.2013.11.043.

Dunai, T.J., 2001, Scaling factors for production rates of in situ produced cosmogenic nuclides: a critical reevaluation: Earth and Planetary Science Letters, v. 176, p. 157–169.

Frankel, K.L., and Dolan, J.F., 2007, Characterizing arid region alluvial fan surface roughness with airborne laser swath mapping digital topographic data: Journal of Geophysical Research, v. 112, p. F02025, doi:10.1029/2006JF000644.

Frankel, K.L., Jayko, A.S., and Glazner, A.F., 2001, Characteristics of Holocene fault scarp morphology, southern part of the Black Mountains fault zone, Death Valley, *in* Machette, M.N., Johnson, M.L., and Slate, J.S., eds., Quaternary and Late Pliocene Geology of the Death Valley Region: Recent Observations on Tectonics, Stratigraphy, and Lake Cycles (Guidebook for the 2001 Pacific Cell, Friends of the Pleistocene Field Trip, Denver, Colorado): U.S. Geological Survey Open File Report 01-51, p. 205–216.

Frankel, K.L., Brantley, K.S., Dolan, J.F., Finkel, R.C., Klinger, R.E., Knott, J.R., Machette, M.N., Owen, L.A., Phillips, F.M., Slate, J.L., and Wenicke, B.P., 2007a, Cosmogenic ^{10}Be and ^{36}Cl geochronology of offset alluvial fans along the northern Death Valley fault zone: Implications for transient strain in the Eastern California shear zone: Journal of Geophysical Research. Solid Earth, v. 112, p. B06407, doi:10.1029/2006JB004350.

Frankel, K.L., Dolan, J.F., Finkel, R.C., Owen, L.A., and Hoeft, J.S., 2007b, Spatial variations in slip rate along the Death Valley–Fish Lake Valley fault system determined from LiDAR topographic data and cosmogenic ^{10}Be geochronology: Geophysical Research Letters, v. 34, p. L18303, doi:10.1029/2007GL030549.

Frankel, K.L., Glazner, A.F., Kirby, E., Monastero, F.C., Strane, M.D., Oskin, M.E., Unruh, J.R., Walker, J.D., Anandakrishnan, S., Bartley, J.M., Coleman, D.S., Dolan, J.F., Finkel, R.C., Greene, D., Kylander-Clark, A., Morrero, S., Owen, L.A. and Phillips, F., 2008, Active tectonics of the Eastern California shear zone, *in* Duebendorfer, E.M., and Smith, E.I., eds., Field Guide to Plutons, Volcanoes, Reefs, Dinosaurs, and Possible Glaciation in Selected Areas of Arizona, California, and Nevada: Geological Society of America Field Guide 11, p. 43–81, doi:10.1130/2008.fld011(03).

Frankel, K.L., Dolan, J.F., Owen, L.A., Ganev, P., and Finkel, R.C., 2011, Spatial and temporal constancy of seismic strain release along an evolving segment of the Pacific–North America plate boundary: Earth and Planetary Science Letters, v. 304, p. 565–576, doi:10.1016/j.epsl.2011.02.034.

Ganev, P.N., Dolan, J.F., Frankel, K.L., and Finkel, R.C., 2010, Rates of extension along the Fish Lake Valley fault and transtensional deformation in the Eastern California shear zone–Walker Lane belt: Lithosphere, v. 2, p. 33–49, doi:10.1130/L51.1.

Guest, B., Niemi, N., and Wernicke, B., 2007, Stateline fault system: A new component of the Miocene–Quaternary Eastern California shear zone: Geological Society of America Bulletin, v. 119, p. 1337–1347, doi:10.1130/0016-7606(2007)119[1337:SFSANC]2.0.CO;2.

Hayman, N.W., Knott, J.R., Cowan, D.S., Nemser, E., and Sarna-Wojcicki, A.M., 2003, Quaternary low-angle slip on detachment faults in Death Valley, California: Geology, v. 31, no. 4, p. 343–346, doi:10.1130/0091-7613(2003)031<0343:QLASOD>2.0.CO;2.

Heisinger, B., Lal, D., Jull, A.J.T., Kubik, P., Ivy-Ochs, S., Knie, K., Nolte, E., 2002a, Production of selected cosmogenic radionuclides by muons: 2. Capture of negative muons: Earth and Planetary Science Letters, v. 200, p. 357–369.

Heisinger, B., Lal, D., Jull, A.J.T., Kubik, P., Ivy-Ochs, S., Neumaier, S., Knie, K., Lazarev, V., Nolte, E., 2002b, Production of selected cosmogenic radionuclides by muons 1. Fast muons: Earth and Planetary Science Letters, v. 200, p. 345–355.

Hoffman, W.R., 2009, Late Pleistocene Slip Rates Along the Panamint Valley Fault Zone, Eastern California [M.S. thesis]: State College, Pennsylvania, Pennsylvania State University, 81 p.

Hooke, R., Le, B., 1972, Geomorphic evidence for late-Wisconsin and Holocene tectonic deformation, Death Valley, California: Geological Society of America Bulletin, v. 83, p. 2073–2098, doi:10.1130/0016-7606(1972)83[2073:GEFLAH]2.0.CO;2.

Hooke, R., Le B., and Dorn, R.I., 1992, Segmentation of alluvial fans in Death Valley, California—New insights from surface-exposure dating and laboratory modeling: Earth Surface Processes and Landforms, v. 17, p. 557–574.

Hunt, C.B., and Mabey, D.R., 1966, Stratigraphy and Structure of Death Valley, California: U.S. Geological Survey Professional Paper 494-A, 162 p., 3 plates.

Keener, C., Serpa, L., and Pavlis, T.L., 1993, Faulting at Mormon Point, Death Valley, California: A low-angle normal fault cut by high-angle faults: Geology, v. 21, p. 327–330, doi:10.1130/0091-7613(1993)021<0327:FAMPDV>2.3.CO;2.

Kirby, E., Burbank, D.W., Reheis, M., and Phillips, F., 2006, Temporal variations in slip rate of the White Mountain fault zone, eastern California: Earth and Planetary Science Letters, v. 248, p. 168–185, doi:10.1016/j.epsl.2006.05.026.

Klinger, R.E., 2001a, Beatty Junction bar complex *in* Machette, M.N., Johnson, M.L., and Slate, J.S., eds., Quaternary and Late Pliocene Geology of the Death Valley Region: Recent Observations on Tectonics, Stratigraphy, and Lake Cycles (Guidebook for the 2001 Pacific Cell, Friends of the Pleistocene Field Trip, Denver, Colorado): U.S. Geological Survey Open File Report 01-51, p. 40–49.

Klinger, R.E., 2001b, Evidence for large dextral offset near Red Wall Canyon, *in* Machette, M.N., Johnson, M.L., and Slate, J.S., eds., Quaternary and Late Pliocene Geology of the Death Valley Region: Recent Observations on Tectonics, Stratigraphy, and Lake Cycles (Guidebook for the 2001 Pacific Cell, Friends of the Pleistocene Field Trip, Denver, Colorado): U.S. Geological Survey Open File Report 01-51, p. 32–37.

Klinger, R.E., 2001c, Quaternary Stratigraphy, Soil Geomorphology, and Tephrochronology of Northern Death Valley—Implications for Tectonic Activity Along the Northern Death Valley Fault Zone [Ph.D. dissertation]: Boulder, Colorado, University of Colorado, 624 p.

Klinger, R.E., and Piety, L.A., 1996, Evaluation and Characterization of the Quaternary Faulting on the Death Valley and Furnace Creek Faults, Death Valley, California (Activity 8.3.1.17.4.3.2): Yucca Mountain Project Seismotectonic Report 96-10, 98 p.

Klinger, R.E., and Piety, L.A., 2001, Holocene faulting and slip rates along the Black Mountains fault zone near Mormon Point, *in* Machette, M.N., Johnson, M.L., and Slate, J.L., eds., Quaternary and late Pliocene geology of the Death Valley region: Recent observations on tectonics, stratigraphy, and lake cycles (Guidebook for the 2001 Pacific Cell—Friends of the Pleistocene Field Trip, Denver, Colorado): U.S. Geological Survey Open File Report 01-51, p. 193–203.

Klinger, R.E., and Sarna-Wojcicki, A.M., 2001, Field trip guide for Day A, northern Death Valley, *in* Machette, M.N., Johnson, M.L., and Slate, J.S., eds., Quaternary and Late Pliocene Geology of the Death Valley Region: Recent Observations on Tectonics, Stratigraphy, and Lake Cycles (Guidebook for the 2001 Pacific Cell, Friends of the Pleistocene Field Trip, Denver, Colorado): U.S. Geological Survey Open File Report 01-51, p. 5–20.

Knott, J.R., and Wells, S.G., 2001, Late Pleistocene slip rate of the Black Mountains fault zone, *in* Machette, M.N., Johnson, M.L., and Slate, J.L., eds., Quaternary and Late Pliocene Geology of the Death Valley Region: Recent Observations on Tectonics, Stratigraphy, and Lake Cycles (Guidebook for the 2001 Pacific Cell, Friends of the Pleistocene Field Trip, Denver, Colorado): U.S. Geological Survey Open File Report 01-51, p. 103–104.

Knott, J.R., Sarna-Wojcicki, A.M., Meyer, C.E., Tinsley, J.C., III, Wells, S.G., and Wan, E., 1999, Late Cenozoic stratigraphy and tephrochronology of the western Black Mountains piedmont, Death Valley, California: Implications for the tectonic development of Death Valley, *in* Wright, L.A., and Troxel, B.W., eds., Cenozoic Basins of the Death Valley Region: Geological Society of America Special Paper 333, p. 345–366, doi:10.1130/0-8137-2333-7.345.

Knott, J.R., Tinsley, J.C., III, and Wells, S.G., 2002, Are the benches at Mormon Point, Death Valley, California, U.S.A., scarps or shorelines?: Quaternary Research, v. 58, p. 352–360, doi:10.1006/qres.2002.2382.

Knott, J.R., Sarna-Wojcicki, A.M., Machette, M.N., and Klinger, R.E., 2005, Upper Neogene stratigraphy and tectonics of Death Valley—A review: Earth-Science Reviews, v. 73, no. 1–4, p. 245–270, doi:10.1016/j.earscirev.2005.07.004.

Kozacı, Ö., Dolan, J.F., and Finkel, R.C., 2009, Late Holocene slip rate for the central North Anatolian fault, Tahtakorpru, Turkey, from Cosmogenic ^{10}Be geochronology: Implications for the constancy of fault loading and strain release rates: Journal of Geophysical Research, v. 114, p. 2009, doi:10.1029/2008JB005760.

Lal, D., 1991, Cosmic ray labeling of erosion surfaces: In situ nuclide production rates and erosion models: Earth and Planetary Science Letters, v. 104, p. 424–439, doi:10.1016/0012-821X(91)90220-C.

Le, K., Lee, J., Owen, L.A., and Finkel, R.C., 2007, Late Quaternary slip rates along the Sierra Nevada frontal fault zone, California: Slip partitioning across the western margin of the Eastern California shear zone/Basin and Range Province: Geological Society of America Bulletin, v. 119, p. 240–256, doi:10.1130/B25960.1.

Lee, J., Rubin, C.M., and Calvert, A., 2001a, Quaternary faulting history along the Deep Springs fault, California: Geological Society of America Bulletin, v. 113, p. 855–869, doi:10.1130/0016-7606(2001)113<0855:QFHATD>2.0.CO;2.

Lee, J., Spencer, J.Q., and Owen, L.A., 2001b, Holocene slip rates along the Owens Valley fault, California: Implications for the recent evolution of the Eastern California shear zone: Geology, v. 29, p. 819–822, doi:10.1130/0091-7613(2001)029<0819:HSRATO>2.0.CO;2.

Lee, J., Stockli, D.F., Owen, L.A., Finkel, R.C., and Kislitsyn, R., 2009, Exhumation of the Inyo Mountains, California: Implications for the timing of extension along the western boundary of the Basin and Range Province and distribution of dextral fault slip rates across the Eastern California shear zone: Tectonics, v. 28, p. TC1001, doi:10.1029/2008TC002295.

Li, J., Lowenstein, T.K., Brown, C.B., Ku, T.L., and Luo, S., 1996, A 100 ka record of water tables and paleoclimates from salt cores, Death Valley, California: Palaeogeography, Palaeoclimatology, Palaeoecology, v. 123, p. 179–203, doi:10.1016/0031-0182(95)00123-9.

Lifton, N.A., Bieber, J.W., Clem, J.M., Duldig, M.L., Evenson, P., Humble, J.E., Pyle, R., 2005, Addressing solar modulation and long-term uncertainties in scalingsecondary cosmic rays for in situ cosmogenic nuclide applications: Earth and Planetary Science Letters, v. 239, p. 140–161.

Lowenstein, T.K., Li, J., Brown, C.B., Roberts, S.M., Ku, T.L., Luo, S., and Yang, W., 1999, 200 k.y. paleoclimate record from Death Valley salt core: Geology, v. 27, p. 3–6, doi:10.1130/0091-7613(1999)027<0003:KYPRFD>2.3.CO;2.

Machette, M.N., 1985, Calcic soils in the southwestern United States, *in* Weide, D.L., ed., Soils and Quaternary Geology of the Southwestern United States: Geological Society of America Special Paper 203, p. 1–22, doi:10.1130/SPE203-p1.

Machette, M.N., and Crone, A., 2001, Late Holocene faulting on the Old Ghost alluvial-fan complex, *in* Machette, M.N., Johnson, M.L., and Slate, J.L., eds., Quaternary and Late Pliocene Geology of the Death Valley Region: Recent Observations on Tectonics, Stratigraphy, and Lake Cycles (Guidebook for the 2001 Pacific Cell, Friends of the Pleistocene Field Trip, Denver, Colorado): U.S. Geological Survey Open File Report 01-51, p. 67–74.

Machette, M.N., Klinger, R.E., Knott, J.R., Wills, C.J., Bryant, W.A., and Reheis, M.C., 2001, A proposed nomenclature for the Death Valley fault system, *in* Machette, M.N., Johnson, M.L., and Slate, J.L., eds., Quaternary and Late Pliocene Geology of the Death Valley Region: Recent Observations on Tectonics, Stratigraphy, and Lake Cycles (Guidebook for the 2001 Pacific Cell, Friends of the Pleistocene Field Trip, Denver, Colorado): U.S. Geological Survey Open File Report 01-51, p. 173–183.

Machette, M.N., Slate, J.L., and Phillips, F.M., 2008, Terrestrial Cosmogenic-Nuclide Dating of Alluvial Fans in Death Valley, California: U.S. Geological Survey Professional Paper 1755, 51 p.

Mann, P., 2008, Global catalogue, classification and tectonic origins of restraining and releasing bends on active and ancient strike-slip fault systems, *in* Cunningham, W.D., and Mann, P., eds., Tectonics of Strike-Slip Restraining and Releasing Bends: Geological Society of London Special Publications 290, p. 13–142.

Meade, B.J., and Hager, B.H., 2005, Block models of crustal motion in southern California constrained by GPS measurements: Journal of Geophysical Research, v. 110, p. B03403, doi:10.1029/2004JB003209.

Mejdahl, M., 1979, Thermoluminescence dating: Beta dose attenuation in quartz grains: Archaeometry, v. 21, p. 61–72, doi:10.1111/j.1475-4754.1979.tb00241.x.

Menges, C.M., Taylor, E.M., Workman, J.B., and Jayko, A.S., 2001, Regional surficial-deposit mapping in the Death Valley area of California and Nevada in support of ground-water modeling, *in* Machette, M.N., Johnson, M.L., and Slate, J.L., eds., Quaternary and Late Pliocene Geology of the Death Valley Region: Recent Observations on Tectonics, Stratigraphy, and Lake Cycles (Guidebook for the 2001 Pacific Cell, Friends of the Pleistocene Field Trip, Denver, Colorado): U.S. Geological Survey Open File Report 01-51, p. 151–166.

Miller, M.G., 1991, High-angle origin of the currently low-angle Badwater turtleback fault, Death Valley, California: Geology, v. 19, p. 372–375, doi:10.1130/0091-7613(1991)019<0372:HAOOTC>2.3.CO;2.

Murray, A.S., and Wintle, A.G., 2000, Luminescence dating of quartz using an improved single-aliquot regenerative-dose protocol: Radiation Measurements, v. 32, no. 1, p. 57–73, doi:10.1016/S1350-4487(99)00253-X.

Nishiizumi, K., Kohl, C.P., Arnold, J.R., Dorn, R., Klein, J., Fink, D., Middleton, R., and Lal, D., 1993, Role of in situ cosmogenic nuclides ^{10}Be and ^{26}Al in the study of diverse geomorphic processes: Earth Surface Processes and Landforms, v. 18, p. 407–425, doi:10.1002/esp.3290180504.

Nishiizumi, K., Imamura, M., Caffee, M.W., Southon, J.R., Finkel, R.C., and McAninch, J., 2007, Absolute calibration of Be-10 AMS standards: Nuclear Instruments & Methods in Physics Research, Section B, Beam Interactions with Materials and Atoms, v. 258, p. 403–413, doi:10.1016/j.nimb.2007.01.297.

Oswald, J.A., and Wesnousky, S.A., 2002, Neotectonics and Quaternary geology of the Hunter Mountain fault zone and Saline Valley region, southeastern California: Geomorphology, v. 42, p. 255–278, doi:10.1016/S0169-555X(01)00089-7.

Owen, L.A., Frankel, K.L., Knott, J.R., Reynhout, S., Finkel, R.C., Dolan, J.F., and Lee, J., 2011, Beryllium-10 terrestrial cosmogenic nuclide surface exposure dating of Quaternary landforms in Death Valley: Geomorphology, v. 125, p. 541–557, doi:10.1016/j.geomorph.2010.10.024.

Pigati, J.S., and Lifton, N.A., 2004, Geomagnetic effects on time-integrated cosmogenic nuclide production with emphasis on in situ ^{14}C and ^{10}Be: Earth and Planetary Science Letters, v. 226, p. 193–205, doi:10.1016/j.epsl.2004.07.031.

Prescott, J.R., and Hutton, J.T., 1988, Cosmic ray and gamma ray dosimetry for TL and ESR: Nuclear Tracks and Radiation Measurements, v. 14, p. 223–227, doi:10.1016/1359-0189(88)90069-6.

Prescott, J.R., Hutton, J.T., 1994, Cosmic ray contributions to dose rates for luminescence and ESR dating: large depths and long-term time variations: Radiation Measurements, v. 23, p. 497–500.

Reheis, M.C., and Dixon, T.H., 1996, Kinematics of the Eastern California shear zone: Evidence for slip transfer from Owens and Saline Valley fault zones to Fish Lake Valley fault zone: Geology, v. 24, no. 4, p. 339–342, doi:10.1130/0091-7613(1996)024<0339:KOTECS>2.3.CO;2.

Reynolds, M.W., 1969, Stratigraphy and Structural Geology of the Titus and Titanothere Canyons Area, Death Valley, California [Ph.D. dissertation]: Berkeley, California, University of California–Berkeley, 310 p.

Rogers, A.M., Harmsen, S., Corbett, E., Priestley, K., and dePolo, D., 1991, The seismicity of Nevada and some adjacent parts of the Great Basin, *in* Slemmons, D.B., Engdahl, E.R., Zoback, M.D., and Blackwell, D.D., eds., Neotectonics of North America: Boulder, Colorado, Geological Society of America, Decade of North American Geology Map Volume 1, p. 153–184.

Rood, D.H., Burbank, D.W., and Finkel, R.C., 2011, Spatiotemporal patterns of fault slip rates across the central Sierra Nevada frontal fault zone: Earth and Planetary Science Letters, v. 301, p. 457–468, doi:10.1016/j.epsl.2010.11.006.

Sheehan, T.P., 2007, Evolution of Neogene Fault Populations in Northern Owens Valley, California and Implications for the Eastern California Shear Zone [Ph.D. thesis]: New Orleans, Louisiana, Tulane University, 203 p.

Sohn, M.F., Mahan, S.A., Knott, J.R., and Bowman, D.D., 2007, Luminescence ages for alluvial fan deposits in southern Death Valley: Implications for climate-driven sedimentation along a tectonically active mountain front: Quaternary International, v. 166, p. 49–60, doi:10.1016/j.quaint.2007.01.002.

Sohn, M.F., Knott, J.R., and Mahan, S.A., 2014, Paleoseismology of the southern section of the Black Mountains and southern Death Valley fault zones, Death Valley, United States: Environmental & Engineering Geoscience, v. 20, no. 2, p. 177–198, doi:10.2113/gseegeosci.20.2.177.

Staiger, J., Gosse, J., Toracinta, R., Oglesby, B., Fastook, J., and Johnson, J.V., 2007, Atmospheric scaling of cosmogenic nuclide production: Climate effect: Journal of Geophysical Research, v. 112, p. B02205, doi:10.1029/2005JB003811.

Staley, D.M., Wasklewicz, T.A., and Blaszczynski, J.S., 2006, Surficial patterns of debris flow deposition on alluvial fans in Death Valley, CA, using airborne laser swath mapping data: Geomorphology, v. 74, v. 152–163.

Stone, J.O., 2000, Air pressure and cosmogenic isotope production: Journal of Geophysical Research, v. 105, p. 23,753–23,759, doi:10.1029/2000JB900181.

U.S. Geological Survey (USGS), 2014, Quaternary Faults in Google Earth: http://earthquake.usgs.gov/hazards/qfaults/google.php (last accessed December 2014).

Volker, H.X., Wasklewicz, T.A., and Ellis, M.A., 2007, A topographic fingerprint to distinguish alluvial fan formative processes: Geomorphology, v. 88, p. 34–45, doi:10.1016/j.geomorph.2006.10.008.

Wasklewicz, T., Mihir, M., and Whitworth, J., 2008, Surface variability of alluvial fans generated by disparate processes, Eastern Death Valley, CA: The Professional Geographer, v. 60, p. 207–223, doi:10.1080/00330120701836162.

Wells, D.L., and Coppersmith, K.J., 1994, New empirical relationships among magnitude, rupture length, rupture area, and surface displacement: Bulletin of the Seismological Society of America, v. 84, no. 4, p. 974–1002.

Wesnousky, S.G., 1986, Earthquakes, quaternary faults, and seismic hazard in California: Journal of Geophysical Research, v. 91, no. B12, p. 12,587–12,631.

Wills, C.J., 1989, A neotectonic tour of the Death Valley fault zone: California Geology, v. 42, no. 9, p. 195–200.

Wright, L.A., 1976, Late Cenozoic fault patterns and stress fields in the Great Basin and westward displacement of the Sierra Nevada block: Geology, v. 4, p. 489–494, doi:10.1130/0091-7613(1976)4<489:LCFPAS>2.0.CO;2.

Zhang, P., Ellis, M., Slemmons, D.B., and Mao, F., 1990, Right-lateral displacements and the Holocene slip rate associated with prehistoric earthquakes along the southern Panamint Valley fault zone: Implications for southern Basin and Range tectonics and coastal California deformation: Journal of Geophysical Research, v. 95, p. 4857–4872, doi:10.1029/JB095iB04p04857.

MANUSCRIPT RECEIVED 21 MAY 2015
REVISED MANUSCRIPT RECEIVED 22 AUGUST 2015
MANUSCRIPT ACCEPTED 10 SEPTEMBER 2015

Printed in the USA

Lithosphere

Timing and rates of Holocene normal faulting along the Black Mountains fault zone, Death Valley, USA

Kurt L. Frankel, Lewis A. Owen, James F. Dolan, Jeffrey R. Knott, Zachery M. Lifton, Robert C. Finkel and Thad Wasklewicz

Lithosphere published online 8 October 2015;
doi: 10.1130/L464.1

Notes